2011

HIGH SPEED CONTINUOUS THERMAL CURING MICROFABRICATION SYSTEM

Franklin DiBartolomeo
University of Kentucky, franklin.dibart@hotmail.com

ABSTRACT OF THESIS

HIGH SPEED CONTINUOUS THERMAL CURING MICROFABRICATION SYSTEM

Rapid creation of devices with microscale features is a vital step in the commercialization of a wide variety of technologies, such as microfluidics, fuel cells and self-healing materials. The current standard for creating many of these microstructured devices utilizes the inexpensive, flexible material poly-dimethylsiloxane (PDMS) to replicate microstructured molds. This process is inexpensive and fast for small batches of devices, but lacks scalability and the ability to produce large surface-area materials. The novel fabrication process presented in this paper uses a cylindrical mold with microscale surface patterns to cure liquid PDMS prepolymer into continuous microstructured films. Results show that this process can create continuous sheets of micropatterned devices at a rate of 1.9 in^2/sec (~1200 mm^2/sec), almost an order of magnitude faster than soft lithography, while still retaining submicron patterning accuracy.

Keywords: Microfabrication, Poly-dimethylsiloxane (PDMS), Microstructures, Microfluidics, Soft Lithography

Franklin DiBartolomeo

4-26-2011

(Date)

HIGH SPEED CONTINUOUS THERMAL CURING MICROFABRICATION SYSTEM

By

Franklin DiBartolomeo

Dr. Christine Trinkle
(Director of Thesis)

Dr. James McDonough
(Director of Graduate Studies)

4-26-2011
(Date)

RULES FOR THE USE OF THESIS

Unpublished theses submitted for the Master's degree and deposited in the University of Kentucky Library are as a rule open for inspection, but are to be used only with due regard to the rights of the authors. Bibliographical references may be noted, but quotations or summaries of parts may be published only with the permission of the author, and with the usual scholarly acknowledgments.

Extensive copying or publication of the thesis in whole or in part also requires the consent of the Dean of the Graduate School of the University of Kentucky.

A library that borrows this thesis for use by its patrons is expected to secure the signature of each user.

Name	Date

THESIS

Franklin DiBartolomeo

The Graduate School

University of Kentucky

2011

HIGH SPEED CONTINUOUS THERMAL CURING MICROFABRICATION SYSTEM

THESIS

A thesis submitted in partial fulfillment of the
Requirements for the degree of Master of Science in Mechanical Engineering in the
College of Engineering at the
University of Kentucky

By

Franklin DiBartolomeo

Lexington, Kentucky

Director: Dr. Christine Trinkle, Professor of Mechanical Engineering

Lexington, Kentucky

2011

TABLE OF CONTENTS

List of Tables..... v

List of Figures..... vi

Chapter One: Introduction
1.1 Microscale Surfaces..... 1
1.2 Research Motivation..... 3
1.3 Summary of Previous Research..... 5
1.3.1 Early Microfludic Fabrication..... 5
1.3.2 Polymer Manufacturing Techniques..... 8
1.3.2A Imprinting and Embossing Polymers..... 9
1.3.2B Injection Molding of Polymer Microchannels..... 12
1.3.2C Soft Lithography..... 13
1.3.2D Roll-to-Roll Nano-Imprint Lithography…….. 16
1.4 Thesis Overview..... 17

Chapter Two: Fabrication Basics
2.1 Machine Overview..... 19
2.2 Preparing the PDMS..... 21
2.3 PDMS Curing Experiments..... 22
2.4 Machine Versions..... 23
2.5 Thermal Analysis of Rolls..... 31
2.6 Embedded Technology..... 34
2.7 Double Sided Patterning..... 36

Chapter Three: Working Parameters
3.1 Mass Flow Rate Balance..... 39
3.2 Roller Speeds..... 43
3.3 Energy Balance..... 48

Chapter Four: Defect Characterization
4.1 Defects Observed, Causes and Solutions..... 52
4.1.1 Surface Defects..... 53
4.1.2 Subsurface Defects..... 61

Chapter Five: Roller Fabrication
5.1 Material Removal Fabrication Techniques..... 62
5.1.1 Micro-Milling..... 62
5.1.2 Micro-Electrical Discharge Machining..... 63
5.1.3 Laser Welding and Milling..... 65
5.1.4 Focused Ion Beam..... 66
5.2 Material Addition Fabrication Techniques..... 67
5.2.1 Electroplating..... 68
5.2.2 Taping..... 69

5.2.3 Wrapping (R2RNIL Method)..... 70
5.3 Recommended Fabrication Technique..... 71

Chapter Six: Conclusions and Future Work
6.1 Conclusions..... 73
6.2 Future Work..... 74

Appendices
Appendix A: Verification of Lumped Capacitance Assumption..... 76
Appendix B: Derivation of Temperature Using Lumped Capacitance Method... 79
Appendix C: Machine Budget..... 82
Appendix D: Orifice Dimensions used in Figure 3-2..... 83
Appendix E: Description of Line Contact Experiment..... 84
Appendix F: Derivation of the radiation heat transfer coefficient..... 85
Appendix G: Roller Design sent for quoting..... 86

References..... 90

Vita..... 93

LIST OF TABLES

Table 5-1, Comparison of each proposed manufacturing technique.....72

LIST OF FIGURES

Figure 1-1, Sequence of photolithographic fabrication on glass..... 6
Figure 1-2, Schematic of Imprinting Methods..... 10
Figure 1-3, Schematic of Hot Embossing Methods..... 11
Figure 1-4, Profilometer Scan of Injection Molded Method..... 13
Figure 1-5, Method of "Soft Lithography"..... 14
Figure 1-6, Roll-to-Roll Nano-Imprint Lithography Schematic..... 16
Figure 2-1, Schematic drawing of the machine..... 21
Figure 2-2, Experimentally determined PDMS thermal curing rates..... 23
Figure 2-3, The 2nd version of the PDMS casting device..... 25
Figure 2-4, Features on the roller..... 26
Figure 2-5, Comparison of Mold and PDMS casting..... 27
Figure 2-6, Micropatterned Cylinders..... 29
Figure 2-7, Schematic of 4th version of the machine..... 29
Figure 2-8, Final version of the continuous-casting machine..... 31
Figure 2-9, Graph of experimental and theoretical cooling of rolls..... 33
Figure 2-10, Medium range resistance heating tape..... 34
Figure 2-11, Materials embedded within the PDMS..... 35
Figure 2-12, Hazards of embedding improper material..... 36
Figure 2-13, Double sided patterning of PDMS..... 38
Figure 3-1, Control volume of process..... 39
Figure 3-2, Experimental verification of hydrodynamic resistance equations..... 42
Figure 3-3, Machine Parameters..... 45
Figure 3-4, Thickness of PDMS membrane vs. Young's Modulus.....47
Figure 3-5, Rollers used for the machine..... 48
Figure 4-1, Surface and subsurface defects..... 52
Figure 4-2, Machine as surface defects are forming..... 53
Figure 4-3, Optical microscopy image of a cross section of a surface defect..... 54
Figure 4-4, Diagram of how surface defects form..... 55
Figure 4-5, PDMS surface defect cause by parallel plates..... 56
Figure 4-6, Pattern of orifices to eliminate surface defects..... 58
Figure 4-7, PDMS without surface defects..... 58
Figure 4-8, Defects caused by improper nozzle geometry..... 59
Figure 4-9, Effect of poor nozzle spacing..... 59
Figure 4-10, Effects of temperature on surface defects..... 60
Figure 5-1, Example of a tool used in micro-milling..... 63
Figure 5-2, EDM capabilities..... 64
Figure 5-3, FIB 3-D capabilities..... 67
Figure 5-4, Microscopy image of roll created by electroplating..... 68
Figure 5-5, Microscopy image of PDMS created using taping method..... 69
Figure 5-6, Creation of roller using wrapping method..... 70

CHAPTER 1 – INTRODUCTION

1.1 Microscale Surfaces

The field of microscale surfaces deals with any engineered surface on the micrometer scale. Under this broad title lies the field of microfluidics which uses those engineered surfaces to manipulate fluids. The majority of applications that find microfluidics useful can be categorized into four general areas: miniaturized analytical systems, biomedical devices, tools for chemistry and biochemistry, and systems for fundamental research [1]. Each area requires one or more of the unique properties that microfluidics can offer. The most obvious of these characteristics is the size of the entire system and the minimal amount of reagents and samples that are needed. However, the fact that fluids in microchannels always exhibit laminar flow [2] is equally important in some cases, as is the optical properties and surface chemistry attained by certain materials manufactured for microfluidics. With all these advantages, it is hard to believe how this field has not been overly commercialized as of yet, however there are a myriad of reasons, one of the most important being the ability to manufacture these devices.

The use of microfluidics is greatly increasing due to the vast number of fields that can use the characteristic properties of fluids in microchannels to their advantage. Microfluidics are being used to help create miniaturized total analysis systems (μTAS) or "lab on a chip" devices. These μTAS can perform analyses up to a factor of 100 times faster than a conventional benchtop system with comparable performance; in one study, this brought the analysis time of demonstrated chip design down into the milliseconds range [3]. Other added bonuses of microfluidics systems are reduced consumption of

reagents and analytes, reduced production of potentially harmful by-products, increased separation efficiency, increased portability, and decreased costs of manufacturing, use and disposal. Also, some studies that cannot be done on a large scale can be done through use of microfluidics. One example is approximating the size and flow conditions found *in vivo* in capillaries. This could lead to research and diagnostic devices of similar size and elasticity as found in biology that could lead to major medical breakthroughs.

In addition to the value of microfluidics, microscale surfaces have other useful applications as well. Sharks have a very unique skin structure that contains dermal denticles. These dermal denticles are small teeth-like structures that are smooth to the touch in one direction and rough in the other. These denticles create tiny vortices in the water, reducing drag and the amount of noise created as a shark swims through the water. The structures are generally about 20 – 30 μm in diameter and spaced 50 μm apart [4]. If this structure could be imitated on the hulls of boats, it could potentially increase the efficiency of the boat. This technology could be tested and brought to life by microstructures if there was a fabrication method efficient and accurate enough to create long strands of a microfluidics device that could be easily sealed to the hull of a boat.

Another potential application for microstructured surfaces is self healing polymers—materials that when damaged can repair themselves via a healing agent and a catalyst. Self healing polymers were designed to repair cracks that form due to mechanical or thermal fatigue which significantly compromises the integrity of the structure. The healing agent is encapsulated within the structure embedded with a catalyst. When a crack propagates through one of the capsules, the healing agent will move through the crack coming into contact with the catalyst and seal the crack. One

study has shown as much as 75% recovery in toughness when this self-healing mechanism was used [5].

One major issue with this type of self healing polymer is that they are essentially single use only. Should another crack propagate through the same spot—which has less than 75% the strength of the surrounding material, making it more likely to fail—the capsules in that area have already been broken and the material cannot heal itself again. However, if material were to contain microchannels flowing with both the healing agent and hardener instead of single-use encapsulated vesicles, the same area could be cracked multiple times before the healing agent would be exhausted in that area. But much like the dermal denticle material, self healing materials generally need to be created in large pieces, which current manufacturing methods are unable to do.

1.2 Research Motivation

Despite the numerous advantages of using microfluidic systems—such as performing chemical and biological analysis in a rapid, portable manner and using smaller volumes of reagents—commercialization of these devices is lagging behind the technology, in large part because of the manufacturing techniques employed. "Soft lithography" [6] is currently one of the most widely used process. It uses photolithography to create a 2-D microstructured mold on a silicon wafer and then replicates that mold using an elastomer such as poly-dimethylsiloxane (PDMS). This technique makes it possible to generate a small number of devices quickly, but since the mold size is inherently limited by the surface area of the silicon wafer—which are

generally 6 inches (152.4 mm) in diameter or smaller—it is difficult to create continuous large surface area patterns.

The goal of the research presented here is to create a novel fabrication method to accurately and continuously replicate microscale designs over a much larger surface area than currently possible. This process is intended to significantly reduce the cycle time needed to create a microstructured device, thereby increasing the commercial feasibility of these devices.

The research described here involves dispensing liquid PDMS prepolymer onto a heated cylindrical mold with a microstructured pattern machined on its surface. While in contact with the mold, the PDMS prepolymer cures on one surface and then comes into contact with another roll to cure and pattern the opposite side. The resulting double sided micropatterned PDMS can be continuously pulled off of the cylinder. This technique can provide high-fidelity microstructured patterns similar to roll-to-roll nanoimprinting lithography [7, 8], but uses a simpler design and can generate monolithic PDMS structures without requiring a poly(ethylene terephthalate) backing. Other advantages of this technology include the ability to perform in-line integration of other components, such as electronics, during PDMS processing. It also enables large scale fabrication of thermoelectric or self-healing materials [5] which require more continuous surface area than a 6 inch (152.4 mm) diameter silicon wafer mold can allow. Trying to create large surface area materials using traditional soft lithography requires that each segment of the material be fabricated separately and then assembled, resulting mismatch and alignment errors between segments. The continuous roller fabrication method proposed here

eliminates the need to assemble a large number of segments because an entire continuous sheet can be fabricated at once.

1.3 Summary of Previous Research

Despite advances in the field of microfluidics, and the wealth of publications in this field, there have been relatively few publications on the fabrication of these devices. Most of the advancements in this area have been techniques adapted from other industries, most notably the integrated circuit industry. The following sections describe many of the microscale fabrication techniques presented in literature. Most of these techniques are batch processing; however, recently there have been some advances in the field of continuous processing.

1.3.1 Early Microfluidic Fabrication

The original microfluidic system was a miniaturized gas chromatography system fabricated on a silicon wafer at Stanford University in 1979 [9]. This system was designed to separate components of a gas mixture into their purest forms; by reducing the internal volume of the chromatography system, this microfluidic chromatography system would only need a minute amount of sample gas to perform the analysis. A typical gas chromatography system consists of a carrier gas, a regulator, the sample gas and injection valve, a capillary column, a thermal conductivity detector and a data processing unit; using microfluidic fabrication, the sample gas injection valve, the capillary column and the thermal conductivity detector were all successfully integrated onto a single 5 cm diameter silicon wafer.

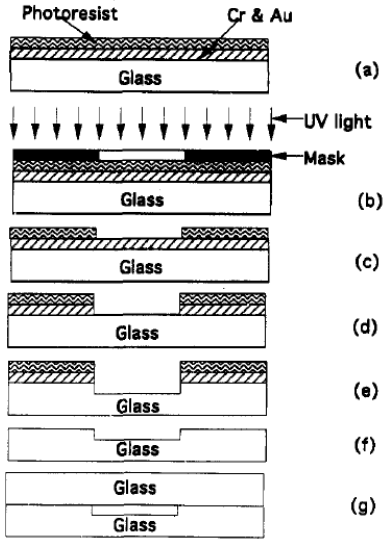

Figure 1-1 - Sequence of photolithographic fabrication on glass. This is very similar to the silicon processing technique: (a) Cr and Au coated glass plate is coated with UV-sensitive photoresist; (b) sample exposed to UV light through a mask; (c) photoresist developed, removing uncrosslinked material; (d) metal exposed through openings in photoresist is removed with a chemical etchant; (e) exposed glass is also etched; (f) resist and metal layers are removed; (g) glass cover plate bonded to form capillary (adapted from [10])

The first step of the fabrication process involved forming a layer of silicon dioxide (SiO_2) on the wafer surface, which would later serve as an etch mask. Next, a standard photoresist and photolithography process was used to define the spiral pattern that would eventually form the microfluidic channels on the front side of the silicon wafer. The wafer was placed in an etching solution and the pattern was isotropically etched into the silicon. This step was repeated and then the wafer was placed in a second solution that would anisotropically etch the silicon to form the input holes. Finally, excess photoresist was stripped from the wafer and it was cleaned and bonded to Pyrex glass. The bonding process consisted of holding the materials together and heating them to 400^{o}C and then applying a 600-V potential between the glass and the silicon. This potential pulled the

wafers and Pyrex into intimate contact and formed an irreversible, hermetic seal, creating a rectangular cross-section capillary channel imbedded in the silicon and Pyrex material.

Most microfluidic devices fabricated in the early 1990s use techniques similar to the one just described; these methods were originally derived from the techniques used to create integrated circuit boards. They were usually fabricated on a glass or silicon wafer using a combination of photolithography and etching steps, such as the example shown in Figure 1-1.

There were two basic ways to produce fluid flow within these devices: using a pressure gradient or electrokinetic pumping [11]. During the early work in microfluidics, electrokinetic pumping [10] was the more popular method, despite the fact that this method forced researchers to use glass or quartz as a substrate material due to the problems caused by the conductivity of silicon during electroosmotic flow. By contrast, modern microfluidic devices tend to rely on pressure-driven pumping, because it is compatible with virtually any material.

Although these methods worked well for research and academic purposes, the methods had certain characteristics that made commercial manufacture of these devices difficult. One was the cost of the substrate material: using silicon or glass wafers costs anywhere from $0.05 to $0.40 per square centimeter. This cost is the same in the microelectronics fabrication, however microfluidic devices are generally designed to be disposable after a single use—necessitating that the production cost be much smaller.

Another barrier to manufacturing is the large number of processing steps and hazardous chemicals involved in photolithographic fabrication. Each wafer must be individually manufactured and processed, which takes time and raises the risk of

manufacturing errors. This drives cost up, as does the disposal of the harmful chemical waste that was created. Channels with high aspect ratios or different height channels are difficult to fabricate using this method in glass or quartz substrates. These types of channels can be formed in silicon, although at a significant price increase due to the cost of silicon. One of the last barriers to manufacturing involved the use of the device itself and the substrate's surface chemistry. Some biomolecules that would be used in a device (oligonucleotides, DNA, or proteins, *etc.*) create unwanted bonds to silicon or glass surfaces. This phenomena could be prevented through use of a surface coating; however, that adds another step to the manufacturing process [12].

1.3.2 Polymer Manufacturing Techniques

Many of the barriers to manufacturing described in the previous section were eventually circumvented through use of polymers as a substrate material. Not only is their cost much lower than that of the quartz, glass and silicon substrates (0.2–2 cents/cm^2), but they also have a wide range of material properties one can choose from depending on the desired use of the device. The late 90's also brought about the development of polymer microfabrication techniques. The reason for this was twofold; one was that the cost for creating silicon based devices was rapidly escalating as was that of the processing equipment; the second was that researchers hoped moving to another substrate might allow for high-volume production of disposable microfluidics devices and open up a commercial avenue for the μTAS concept [12]. However, as of the writing of this paper, the commercialization of disposable microfluidics has been limited mainly to the healthcare field.

The polymers lend themselves to a wide variety of manufacturing techniques such as casting, molding, laser ablation and micromachining. The polymers chosen can have varying properties of thermal and chemical resistance, melting temperature and surface chemistry [13]. Some of the first polymer microfluidic devices were made using poly(methylmethacrylate) (PMMA), however, poly(dimethylsiloxane) (PDMS) is currently more widely used in microfluidics.

1.3.2A Imprinting and Embossing Polymers

The imprinting method was one of the earliest methods of creating microchannels in a polymer. It was done in one of two ways. The first way was simply done by using a wire of a known thickness that was stretched taut and pressed it into the polymer. This assembly was then placed in the oven and heated to the softening temperature of the polymer (Figure 1-2a) [13]. The drawback to this method was that only straight channels could be formed and producing crossing channels required two separate pieces of polymer created simultaneously as they could not accurately produce crossing channels on the same piece of material. Researchers attempted to do it using several iterations of using wire to create the crossing channels. But due to the fact that the polymer is not easily deformed and became even more rigid following the heating cycle, the same blank could not have all the channels needed for a device [13].

The second way to use imprinting methods was slightly more complicated, yet yielded better results and could be used with much more complicated patterns. A layout of the desired microfluidic channels was created using a CAD program. The designs were then printed on a transparency which was used as a mask for photolithography. An oxide layer was then grown on a silicon wafer and then a layer of photoresist was spincoated

onto the oxide and exposed to UV light through the transparency. This removed the photoresist everywhere except where the channels were desired. The wafer was then placed in an HF solution to etch the exposed oxide layer. The photoresist was then removed and the oxide layer left was used as a mask to etch the silicon. After the silicon was etched what was left was a raised area everywhere the channels were desired. Then, similar to what was done with the wires, the silicon master was pressed against the PMMA and put into the oven (Figure 1-2b) [13]. This process yielded good results, however, it takes a long time and access to silicon processing equipment to produce the mold, which may make it difficult to use this process commercially.

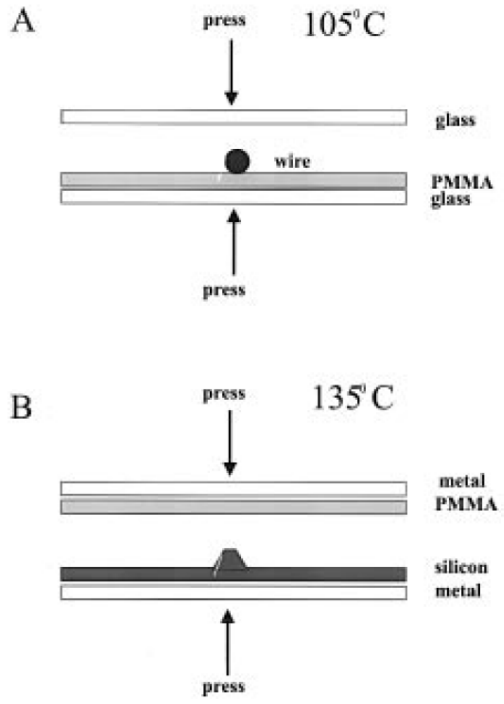

Figure 1-2 - Schematic of Imprinting Methods. Adapted from [13].

Hot embossing is a very similar process to imprinting. It requires a mold being pressed into a polymer substrate, however, with hot embossing, both the mold and the

substrate are heated separately in a vacuum to the glass transition temperature of the substrate prior to being pressed together (See Figure 1-3). They are then held together with a 20 – 30 kN force for 30 – 60 seconds until the system is cooled to just below the glass transition temperature of the substrate. At this point the force is removed and the substrate has the desired channels. This method is quicker than the imprinting methods and can be automated, since similar methods are already in use in the commercial world.

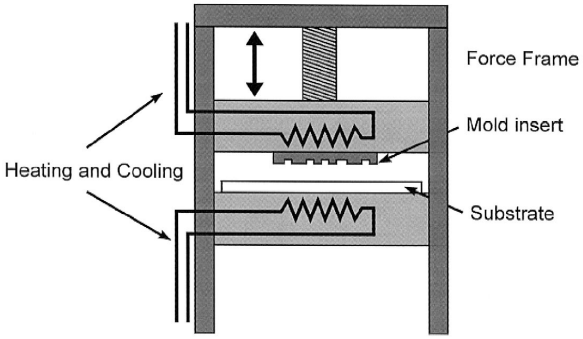

Figure 1-3 - Schematic of Hot Embossing Methods. Adapted from [14]

One of the downsides to this method is in the creation of the mold itself. There are three basic methods and all are relatively time intensive; micromachining using conventional CNC machines, silicon processes using wet or dry etching, and high resolution techniques using LIGA (lithography, electroforming and molding process). The conventional CNC machines are expensive, the LIGA process also calls for a lot of overhead and the etching techniques require a clean room and the use of hazardous chemicals [14]. Another potential drawback to this system is the fact that perfectly vertical walls and undercuts are not attainable. Since the mold is being pressed straight down into the polymer, it is impossible to get an undercut, however this could be achieved by sealing it to another blank. The perfectly vertical walls are unattainable

because when the mold is being pulled from the blank vertical walls would create a sticking friction along the sides and ruin the device. There needs to be some sort of angle on the walls to stop this from happening.

1.3.2B Injection Molding of Polymer Microchannels

Another way to create polymer microfluidic devices is to use the injection molding process. Molds are made by using a wet etching process to form a negative of the channels desired on a silicon blank and then from that a nickel electroform "mother" was created. This mother was a positive of the channel imprint and from this numerous "daughters" of nickel electroform were made. These "daughters" were then used as the mold insert for the injection molding process. The multistep process to produce the mold was created to avoid having to wet etch a silicon blank for every mold insert that was desired, which can be a very intensive process depending on the depth of the etch. Although creating the "daughters" is an extra step, it alleviated the need to constantly use a clean room to create numerous molds from the silicon blank because the process of injection molding causes wear on the molds used.

One benefit of using injection molding is that it is already a widely used method within the commercial world. However, the sealing of the channels caused major issues that had already been resolved with other substrates. Also, the profile of the final channels only loosely followed the profile of the "daughters" due to shrinkage during the cooling phase of the process. Figure 1-5 clearly shows the desired channels compared to the channels created in the acrylic using this method [15]. The reduced accuracy of this method is one of the major reasons this method has been largely unused in the field.

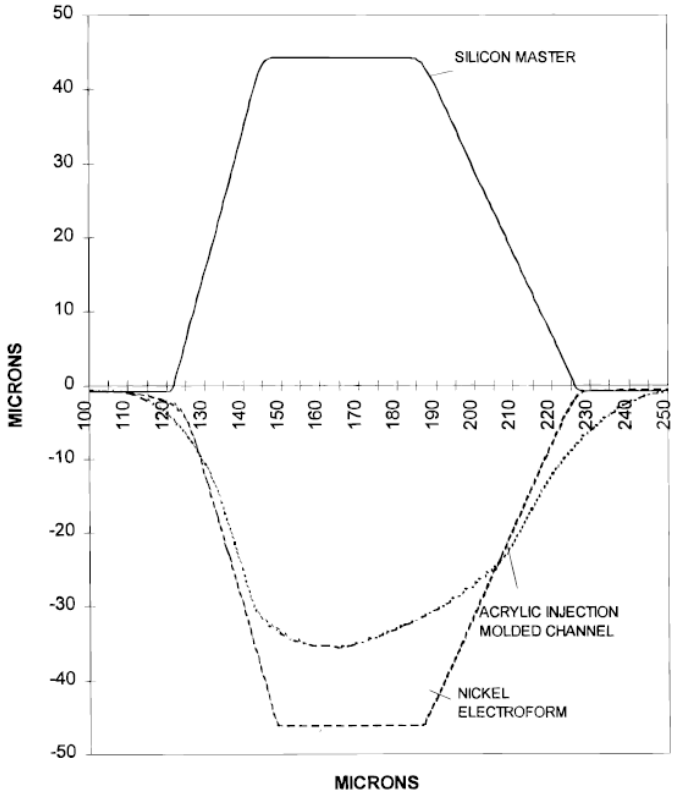

Figure 1-4 - Profilometer scan of injected molded method. The silicon master, the nickel electroform mother and the injection molded acrylic channel can all clearly be seen. Adapted from [15].

1.3.2C Soft Lithography

Currently, one of the most widely used process for creating microfluidic devices is known as "Soft Lithography", which uses a soft elastomeric polymer, typically PDMS. The process has several major advantages: it doesn't require a clean room for the actual replication stage, has a reusable mold, and has a quick turnaround time for new designs. As described in Figure 1-5, the process starts using a photomask created from a CAD file for photolithography on a silicon ship coated with photoresist. This process creates the master which is then used as a mold against which PDMS is cast to create the desired device [6].

PDMS has several unique characteristics that make it an extremely attractive option for the production of microfluidic devices. One is due to the fact that it is transparent, optical detection methods will work. The substance is gas permeable and nontoxic making it appropriate for cellular studies. One potential drawback is that the chemical structure of PDMS leads it to have a hydrophobic surface, but this can easily be made hydrophylic by exposing the surface to an oxygen or air plasma.

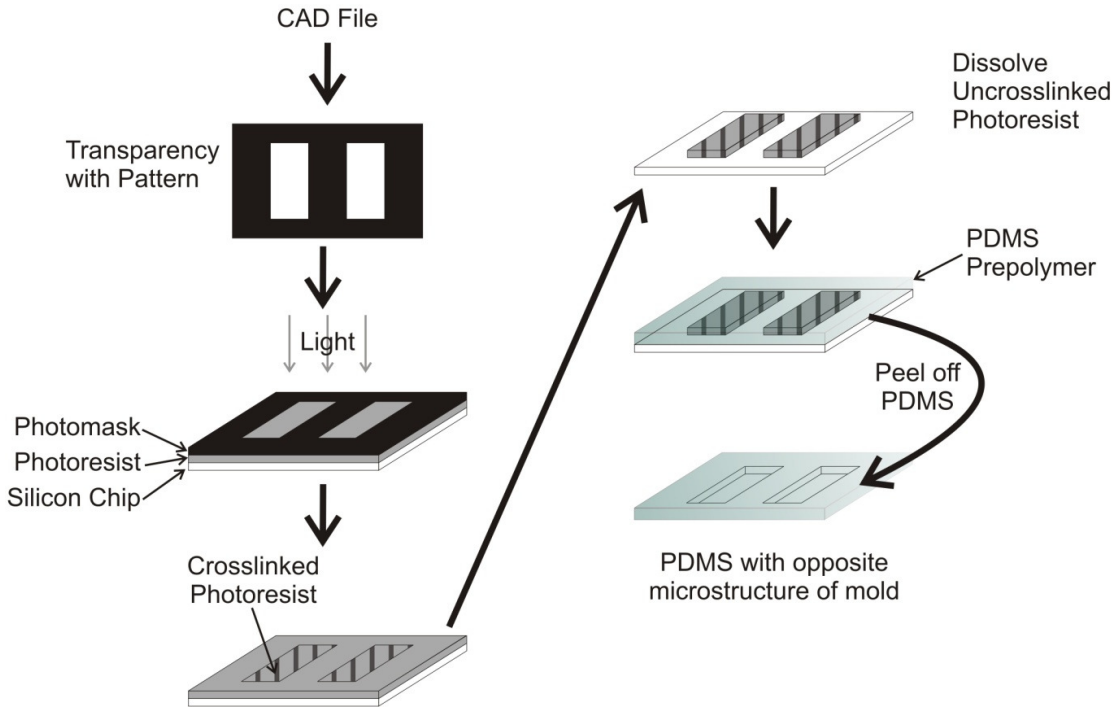

Figure 1-5 – Method of "soft lithography". The pattern starts as a CAD file which is used to create a photomask for photolithography of a photresist on silicon. The silicon is then used as a master mold for creating PDMS with microstructures on its surface.

Although all the previous materials used in the field could be sealed, PDMS is by far the easiest and most adaptable to many situations. PDMS can form an irreversible seal with PDMS, glass, silicon, polystyrene, polyethylene, or silicon nitride by exposing both

the surface of PDMS and the surface of the substrate to an air or oxygen plasma [1]. Exposing both surfaces to oxygen plasma forms covalent –O-Si-O-bonds when the surfaces are brought into contact with each other. By contrast, sealing glass to glass or silicon to silicon requires either high temperatures (~600^{o}C – 800^{o}C) or voltages (~500-1500 V). PDMS also has the ability to be reversibly sealed to any smooth surface via van der Waals or conformal contact. This is useful when patterning surfaces with proteins, cells or biomolecules using fluid flow. The PDMS can also be reversibly sealed to silicone adhesive tape reversibly [16]. The bond to the tape is slightly stronger than the bond to other surfaces and the tape is flexible. The fact that it is a lot easier to cut holes for reservoirs and incorporate filter papers for various reasons is yet another reason to reversibly seal the device to silicone adhesive tape.

Although PDMS has numerous advantages over the previous substrates used for microfluidics, it does have some disadvantages as well. As stated earlier, PDMS is hydrophobic, however, some experiments have found this to be a useful characteristic through protein stamping [17]. PDMS also has a relatively low modulus of elasticity, making it difficult to use in applications needing rigid structuring or unyielding walls at high pressures. Despite these characteristics, PDMS is still regarded as one of the most useful materials when performing microfluidics research. Its ability to be molded in non-clean room conditions and the ability to quickly change a design put it above many other substances used in the past.

1.3.2D Roll-to-Roll Nano-Imprint Lithography

Despite the fact that most of the research into fabrication techniques has been based on batch processing, there have been individuals who have tried to create processes for continuous output of these devices. Roll-to-roll nanoimprint lithography (R2RNIL) [7, 8] is one of these techniques. As seen in Figure 1-6, this process works by coating a sacrificial layer (usually a strip of polyethylene terephthalate, PET) to a specific thickness with either PDMS for a thermal cure or an epoxysilicone for a UV cure. This coated material is then rolled over a cylindrical mold while the PET backing is exposed to either a heat or UV source to cure the substrate.

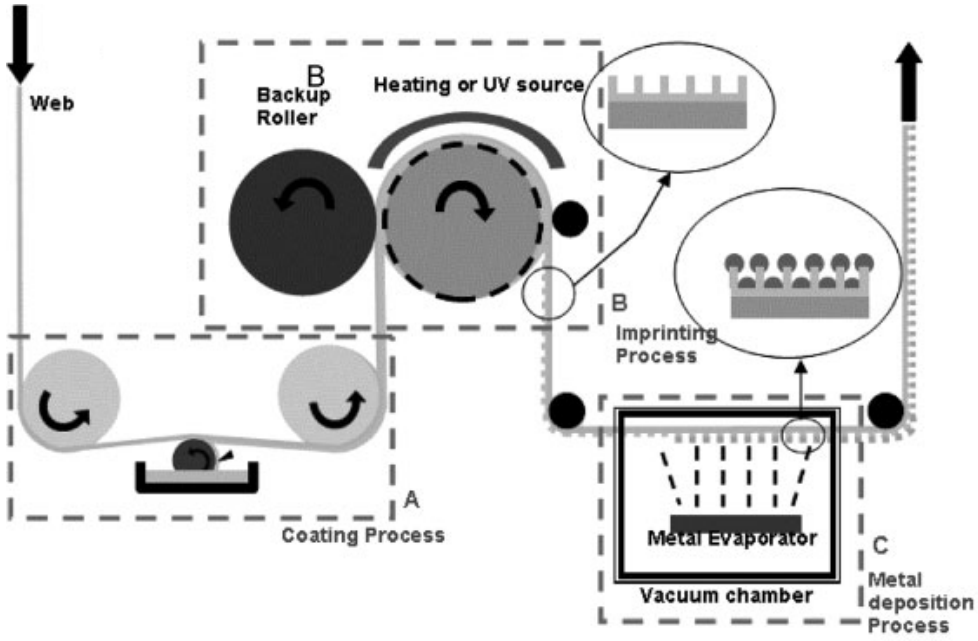

Figure 1-6 – Roll-to-roll nano-imprint lithography schematic. A webbing is coated to a certain thickness and then that coating is imprinted and cured. This process also included evaporating metal onto the pattern for their research purposes, however that final step is optional. Adapted from [7].

Although R2RNIL is one of the first roll to roll processes for creating microfluidic devices, it is not without its drawbacks. It is a very complicated system with numerous rollers and moving parts, therefore, a trained operator is needed to run this machine. Also, the substrate, be it PDMS or epoxysilicone, can only be coated to a certain thickness on the PET backing before it drips off on the way to the mold. Another obvious drawback is that there is a PET backing at all times and monolithic strips cannot be made.

1.4 Thesis Overview

This thesis covers the development of a novel technique of producing PDMS microstructured devices at a much faster rate over traditional soft lithography. The technique developed here uses heated roller molds with microscale surface features to produce continuous sheets of microstructured PDMS. This machine creates monolithic sheets of PDMS and has the capability to pattern both sides of the PDMS if desired.

This paper will outline the proof of concept for the device created and overview the process for replicating it. Chapter 2 describes early experimental work and versions of the machine. This chapter also lays out the total capabilities of the machine. Chapter 3 covers a thermodynamic analysis of the fabrication process, including a mass flow balance, running speeds and input heat energy needed. Chapter 4 probes early issues that affected the surface quality along with the solutions to these problems. Chapter 5 examines different techniques for manufacturing the roller molds for the system; this

section discusses the capabilities and financial impact of each technique. Finally, chapter 6 draws conclusions along with possible future work to be done on the system.

CHAPTER 2 – FABRICATION BASICS

2.1 Machine Overview

Although there have been numerous manufacturing methods used to create microstructures on the surface of substrate, most of these methods are not optimal for commercialization purposes. The early methods of etching silicon and glass [9] were primarily concerned with the ability to create a single microfluidic device, not the ability to mass-produce such a device. Although glass has properties that make it desirable for microfluidic work, such as optical transparency and biological inertness, the high processing cost of glass caused researchers to experiment with polymers for microfluidic applications.

One of the first polymers used in microfluidics was Poly(methyl methacrylate), or PMMA, due to the fact that it has optical transparency similar to glass. With PMMA, many well-established commercial fabrications methods, such as hot embossing [13, 14] and injection molding [15], could be adapted from the plastics industry. However, issues with low replication accuracy and long cycle times still need to be addressed for these methods to be applicable for this type of work. It is clear that advancements were going to be needed not only in the area of manufacturing techniques, but selecting a substrate that is compatible with commercially viable manufacturing methods as well.

The Whitesides group discovered that the elastomer Polydimethylsiloxane (PDMS) also had desirable properties, such as biological inertness, optical transparency and fast curing. Using this material, they developed “soft lithography” [16]: one of the most widely used procedures for creating microfluidic devices in a lab environment. In

this process, a mold is created using photolithography on a silicon wafer with a photoresist and then liquid PDMS is then cured over this mold to create the final device. Although this procedure works very well for small batches, the cycle time to create a device—around 45 minutes to create one wafer of devices—is too slow for many commercial applications. Also, soft lithography cannot produce any devices larger than the mold used to create them; traditionally molds are fabricated on a silicon wafer which is typically less than 6 inches in diameter. This means that large surface area materials can be very difficult to create using soft lithography.

The research presented in this thesis covers the development of an alternative means of producing PDMS microstructured devices. The technique developed here can produce continuous sheets of microstructured PDMS at a rate of 1.9 in^2/s, a five-fold improvement over traditional soft lithography (~0.4 in^2/s for a 6"-diameter wafer). This machine creates monolithic sheets of PDMS and has the capability to pattern both sides of the PDMS. It is currently set up to produce 1 in wide sheets, however, it could be reconfigured for greater width if desired.

The machine uses the quick thermal curing properties of PDMS, combined with microstructured rollers to create sheets of microstructured PDMS. As seen in Figure 2-1, liquid PDMS prepolymer is funneled through a nozzle designed for the specified flow rate onto the first of two heated cylindrical molds. On this roller, one side of the PDMS will cure before it comes into contact with the second roller—which can also be patterned for double sided patterning—to finish the curing process. From there, the PDMS is continuously removed from the second roller.

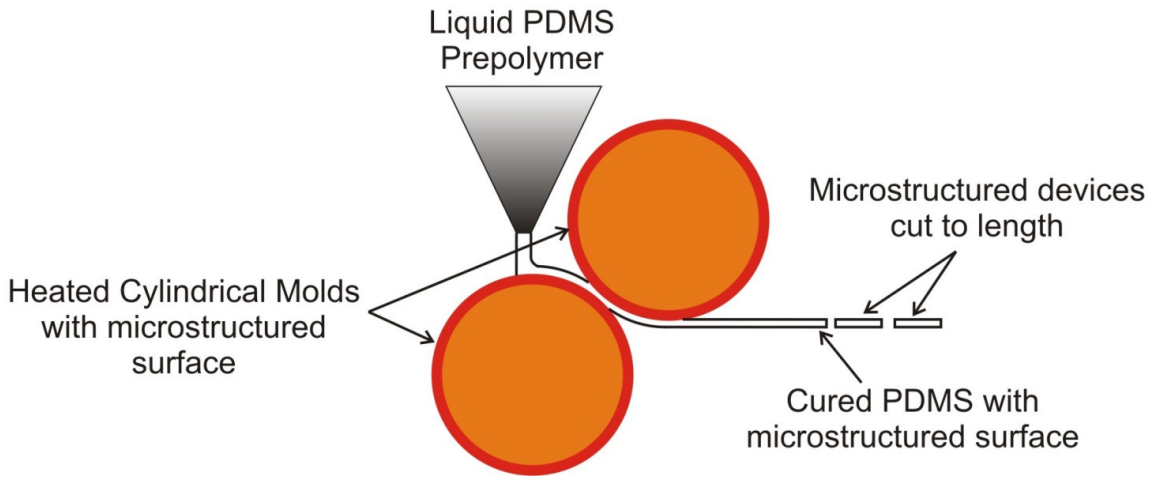

Figure 2-1 – Schematic drawing of the machine. Degassed liquid PDMS prepolymer is loaded into the dispenser and fed into the machine through a nozzle. The PDMS is cured, demolded from each roller and then cut to length depending on the user's requirements.

2.2 Preparing the PDMS

The PDMS used for all of the experiments is Sylgard 184 (Dow Corning), which is packaged in two parts: a base and a curing agent. Mixing these in a weight ratio of 10:1 (base: curing agent) produces the standard product as recommended by Dow Corning. Due to the base being an extremely viscous substance (5000 cP [18]) similar to honey, one must be thorough in mixing in the curing agent to ensure that the reaction between them will occur homogenously. During this phase, air bubbles appear in the matrix and must be removed to prevent defects throughout the PDMS. This can be accomplished by placing the mixture in a centrifuge or more commonly by placing the mixture under vacuum until all the bubbles are removed in a process known as degassing. After this stage, the PDMS is ready to be cured using the method of choice: this is prepolymer will cure at room temperature, or it can be significantly sped up with the addition of heat.

Although degassing removes the majority of air bubbles from the PDMS prepolymer, bubbles can be reintroduced during handling of the liquid in subsequent steps. This reintroduced air causes defects within the material. These defects and methods to minimize them are explained more thoroughly in Section 4.1.2.

2.3 PDMS Curing Experiments

For this system, it was necessary to determine the rate at which PDMS cures in order to determine if the process of creating devices with this material could be made faster. To accomplish this task, PDMS was cured at multiple thicknesses and temperatures to see how the long each took to be completely cured. Sylgard 184 prepolymer starts as a viscous liquid and becomes an elastomer after curing; during the curing process, the PDMS material will have a combination of properties somewhere in between these two states. For the purpose of these experiments, cured was defined as the point at which the PDMS no longer permanently deformed from less than 1 lb of force on its surface. From these experiments, it was found that Sylgard 184 could be cured at a much faster rate than that suggested by its manufacturer: 45 minutes at 100^{o}C [18]. Not surprisingly, the curing rate was proportional to the thickness and inversely proportional to the temperature as shown in Figure 2-2.

Another result of these early experiments was the determination that PDMS could absorb significant heat before it acquired a permanent set. This meant that the prepolymer could be preheated or partially cured before it is cast against the final desired surface. This finding is very critical in the design of the manufacturing process because it meant that the liquid PDMS could be somewhat cured before coming into contact with the final

mold. By preheating the PDMS prepolymer, the amount of time the PDMS had to be in contact each mold could be greatly reduced, making the overall process faster and more efficient.

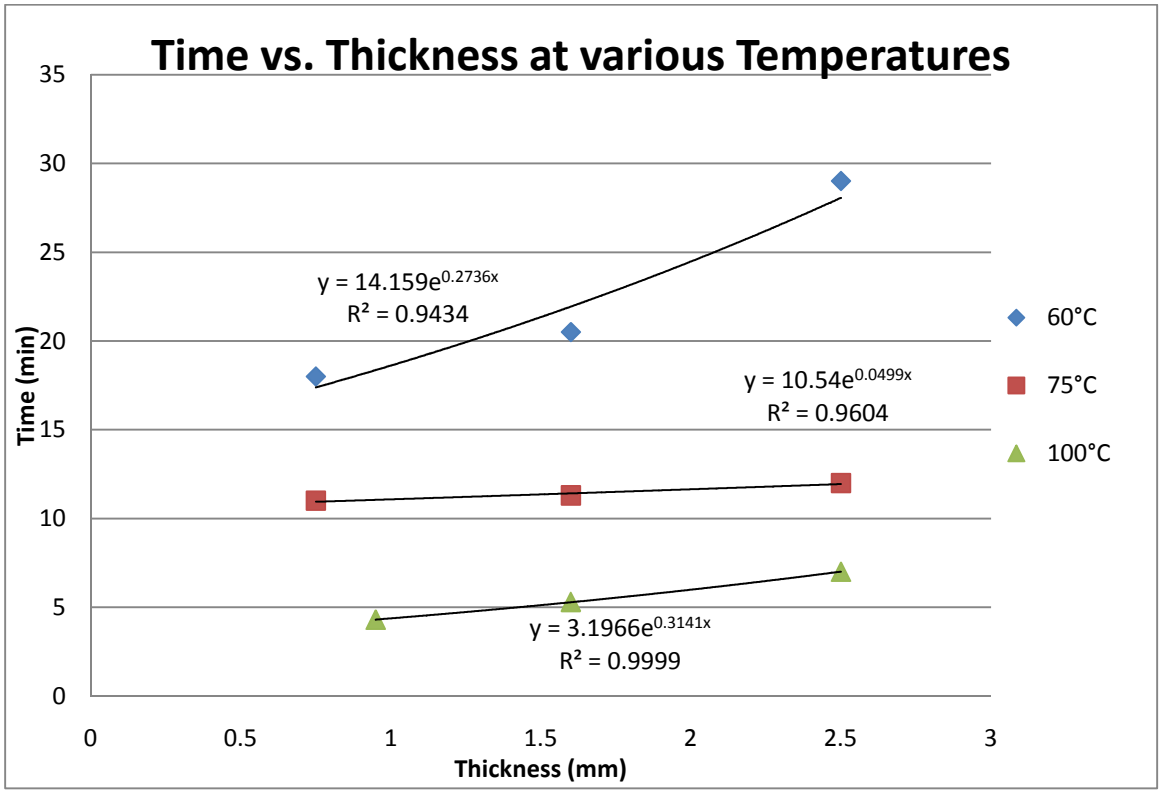

Figure 2-2 – Experimentally-determined PDMS thermal curing rates; results show strong relationships between thickness and time to cure at various temperatures.

2.4 Machine Versions

The initial PDMS thermal curing experiments supported the hypothesis that a continuous output process for curing PDMS could be created. A roller system—like the one developed here—is already widely used in many other processes, such as the continuous casting of steel and laser printing. In this system, an internally heated cylinder containing microstructures on its outer surface was designed to cure the PDMS. For the

first version of the machine, a modified fuser assembly from a laser printer was adapted for the process and used as the roller and heat source. Replicating curing results from oven and hot plate tests was not possible as the prepolymer spilled from the roller before curing had occurred. This problem was solved by "pre-curing" the polymer on a heated ramp that it flowed over before it came into contact with the roller.

For the second version of the machine, the 1.19" diameter roll of the fuser was replaced with a machined 3" diameter aluminum roll, as seen in Figure 2-3. This change was made to facilitate heat transfer from the ceramic heat lamp; the roller also included height variations to allow various thicknesses of PDMS to be created simultaneously. From this version, cured sheets of PDMS measuring 1" X 24" with a thickness of 0.05" were created; the length of these sheets was only limited by the amount of PDMS used during fabrication.

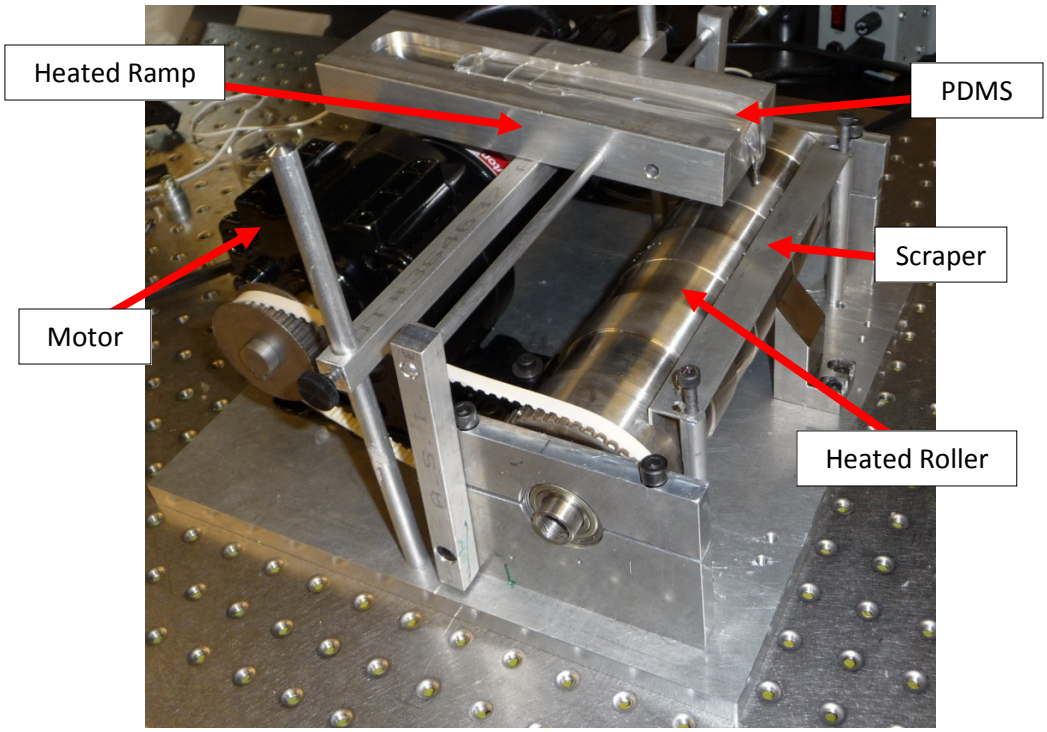

Figure 2-3 – The 2nd version of the PDMS casting device. This version has an aluminum milled roller turned by a DC motor with a preheated ramp for the degassed PDMS prepolymer.

The roller used in the second version of the machine did not have microscale surface features machined on it. However, when the machine was run, the telltale machining marks of the lathe were nearly perfectly replicated onto the sheets of PDMS. Features were then added to the roller surfaces using a traditional end mill; these designs included circles and lines (horizontal, vertical and angled), shown in Figure 2-4. These features were successfully replicated onto the PDMS sheets in subsequent trials and then compared to the roller geometry using data from a white light profilometer (Zygo NewView 5000). As seen in Figure 2-5, the surface topography of the cylinder and the PDMS features are virtually indistinguishable. This demonstrated the accuracy of the

roller-curing process, but the feature size was quite large (0.04” diameter circles) compared to most microstructures.

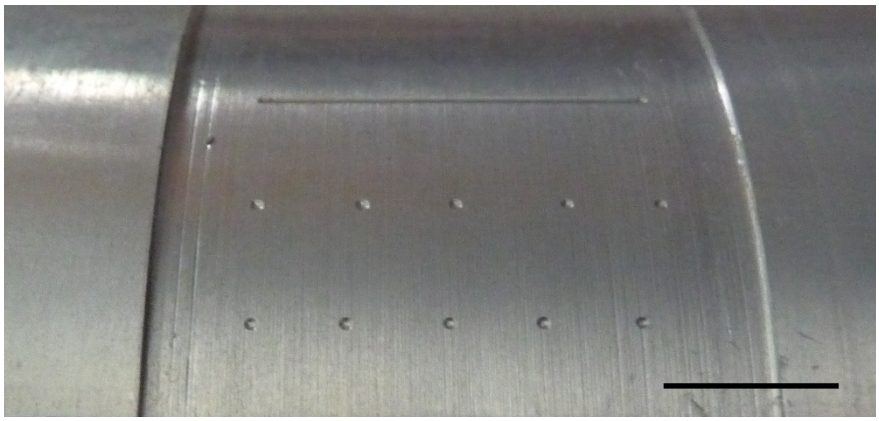

Figure 2-4 – Features on the roller. This version of the roller contained circles and lines created through a traditional machining process using small tools. Scale bar = 0.25”

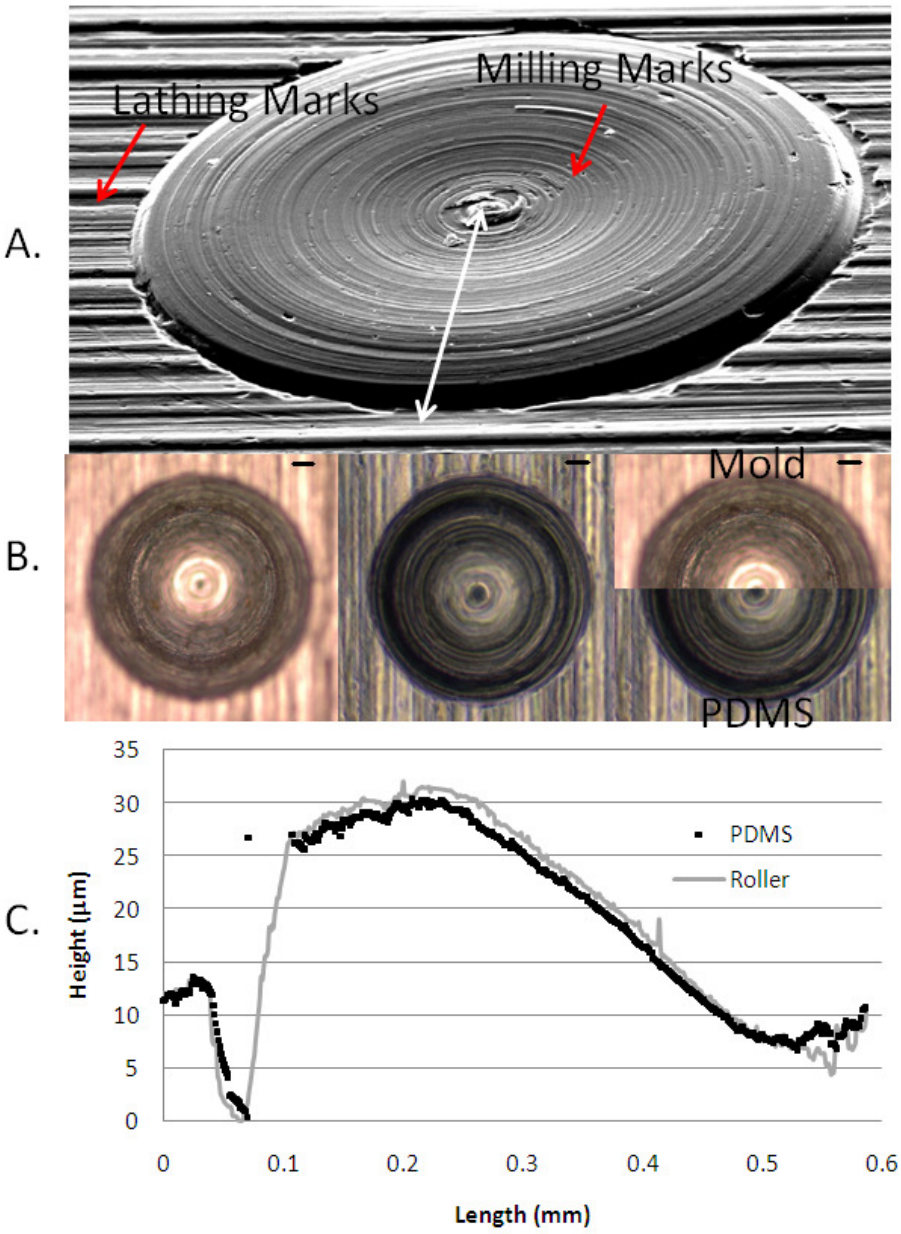

Figure 2-5 – Comparison of mold and PDMS casting device. A) SEM image of PDMS produced by this process with structures of ~0.04 in (1 mm) in diameter. The white line indicates the location of the profilometer scan in the graph below it. B) Image 1 is an optical micrograph of the roller and image 2 is of the PDMS portion that was cast against it. Image 3 is a combined view of image 1 and image 2 demonstrating the high fidelity of the process. Scale bar represents 100 µm. C) Comparison of profilometer scans of a section of patterned PDMS and the corresponding feature on the cylindrical mold. The gap in data and outlier point in the PDMS trace is a result of that portion not being reflective enough for the white light profilometer to read. Adapted from [19].

To attain smaller features, the method of roller fabrication had to change since traditional milling tools could not create the feature sizes needed for most microfabrication applications. A modified LIGA process [20] was available at the University of Kentucky, so this process was selected for testing. Many attempts were made to create a 3" diameter electroplated roller; however, the in-house process was not compatible with a roller of this size. Instead, a third version of the continuous-casting machine was created in order to use larger diameter rolls that could be created with the available LIGA setup, as seen in Figure 2-6.

The change forced by the use of these LIGA-fabricated rolls now allowed the thickness of the cured PDMS to be varied by how close the scraper mechanism was to the rolls. This scraper mechanism was a piece of aluminum used to regulate maximum PDMS thickness and assure PDMS spread to entire width of roll, as shown in Figure 2-3. The other change forced by the use of the rolls was to move away from internal heating due to the difference of internal diameter of the rolls (0.25" vs 4.5"). The mounting and connecting hardware of the ceramic lamps is made of plastic and would melt at 221^{o}C [21], before they were able to heat the new roller to the needed internal temperature to produce an outer temperature of 190^{o}C. The decision was made to heat the roll in the oven to the desired temperature and use the heat capacitance of the stainless steel to cure the PDMS. Although this change worked for testing purposes, internal heating will be needed for a manufacturing environment and is outlined in section 2.5.

Despite the fact good results were created using the scraper mechanism on the rolls with pockets, the scraper was not producing consistent results on the back side of the PDMS. The "flat" surface of the PDMS was curing with undulations and other

inconsistencies. This led to adding another roller so the PDMS would cure between rollers. Since an identical width roller was needed, it was only natural to use another of the electroplated bearing rings to give the ability to pattern both sides of the PDMS. The machine schematic of this version can be seen in Figure 2-7.

Figure 2-6 – Micropatterned cylinders. Originally designed as bearings, these cylinders with micropatterned surfaces served as the rollers for this machine.

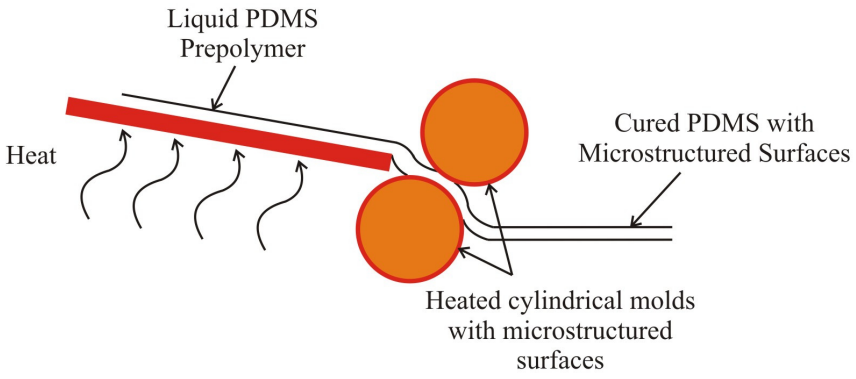

Figure 2-7 – Schematic drawing of the 4th version of the machine. Liquid prepolymer continually flows down a heated path toward two cylindrical molds that finish the curing process. Cured PDMS with microstructured surface is then continually pulled off at the end of the process.

With experimental use, it was obvious that a redesign of the system was needed to ensure ease of use and replication accuracy, leading to the final version shown in Figure 2-8. The new parts were machined out of aluminum billet to tight perpendicularity and parallelism tolerances to hold the rolls. With this major upgrade, other minor issues were addressed as well. One such issue was using bigger bearings to open up the possibility of going back to internal heating, discussed late in Section 2.5. This design allows the user to adjust the roll to roll distance through use of a precision microstage and micrometer. From the micrometer reading and knowledge of the center to center height difference of the rolls, a simple geometric calculation will give the user the distance between the rolls which is also the thickness of the cured PDMS through the system.

Although microstructures were consistently being replicated on the twin roller machine, the system was not complete as the flowrate of the liquid prepolymer was still controlled manually. A hopper and nozzle design was created, as shown in Figure 2-8, to create a steady, consistent flow of PDMS prepolymer into the system. Acrylic was chosen as the nozzle material due to the availability of a laser-cutting system (Versa Laser) that could easily cut acrylic and allow quick change of nozzle sizes between trials. However, use of acrylic forced the system to discontinue use of the heated ramp due to its low melting temperature. There was no way to change the curing characteristics of Sylgard 184, so the decision was made to significantly increase the temperatures of the rollers to keep the same output rate.

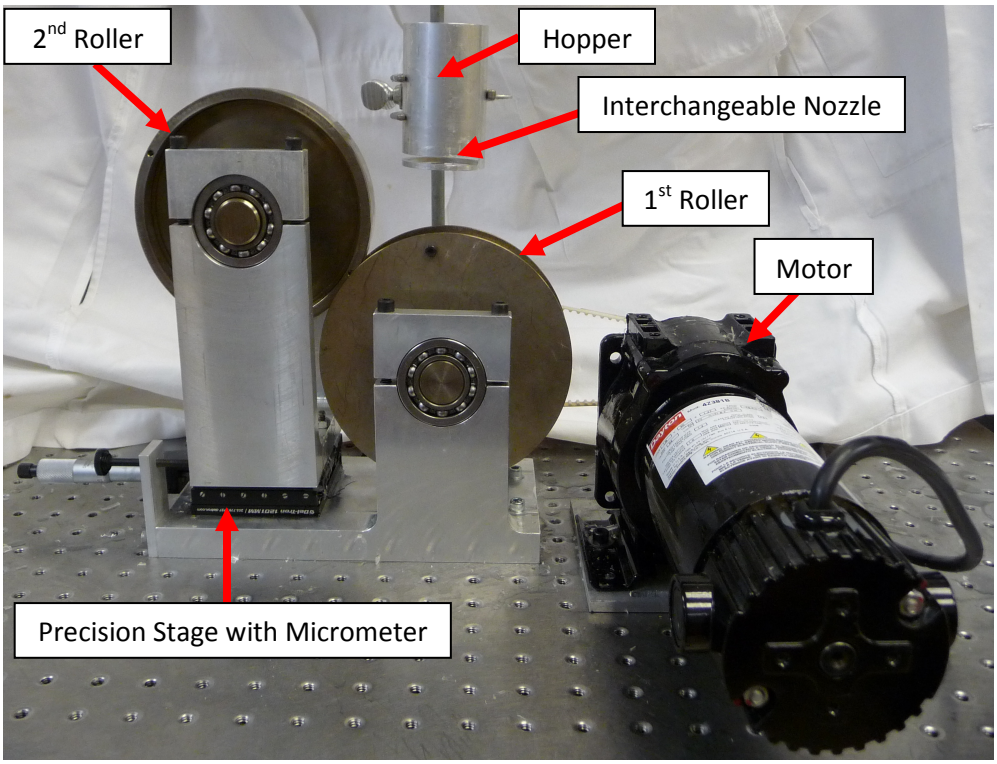

Figure 2-8 – Final version of the continuous-casting machine.

2.5 Thermal Analysis of Rolls

Design and initial testing of the machine took place with a roll that was internally heated by a ceramic lamp heater, similar to how a laser printer roller is heated. However, later versions of the machine used rolls with a large inside diameter and short overall length, which would not accommodate the ceramic lamp heater. Instead, the rollers were heated in an oven before trial runs of the machine. Although using the heat capacitance of a conductor like stainless steel could be potentially unpredictable, as the ambient temperature will play a role in the cooling, data was taken experimentally to measure the cooling rate of the rolls during use. The rollers were heated in an oven until they stabilized at 190°C and then moved to ambient lab conditions; the temperature decrease

was measured using a Fluke Digital Thermometer which has an accuracy of +/- [0.05% + 0.3°C] at temperatures above 100°C and +/- [0.20% + 0.3°C] below 100°C.

The cooling rate of the rollers can also be modeled analytically; equation 2-1 shows that a lumped capacitance approach is valid for this system because the Biot number is less than 0.1:

$$Bi = \frac{hL_c}{k} = \frac{7.45\,{}^{W}/_{m^2K} * 0.00556m}{18.2\,{}^{W}/_{mK}} = 0.002276 \qquad (2\text{-}1)$$

Where h is the heat transfer coefficient, L_c is the characteristic length and k is the convective heat transfer coefficient. For a more detailed analysis, see Appendix A. Applying the lumped capacitance assumption to the rollers, a cooling curve can be derived in the form of Equation 2-2.

$$T(t) = 296K + (177K)e^{-0.000804t} \qquad (2\text{-}2)$$

Plotting this equation against experimentally measured data produces Figure 2-9, which displays the roll temperature versus time. It is shown that the rates of cooling found theoretically and experimentally are almost identical. Based on this data, it was decided to keep the experimental run times for the machine short, typically around 30 seconds or less depending on the rpm desired. Runs typically started at 190°C and from the data, one can see that the rolls cool about 5° C during that time, which is small enough to consider negligible.

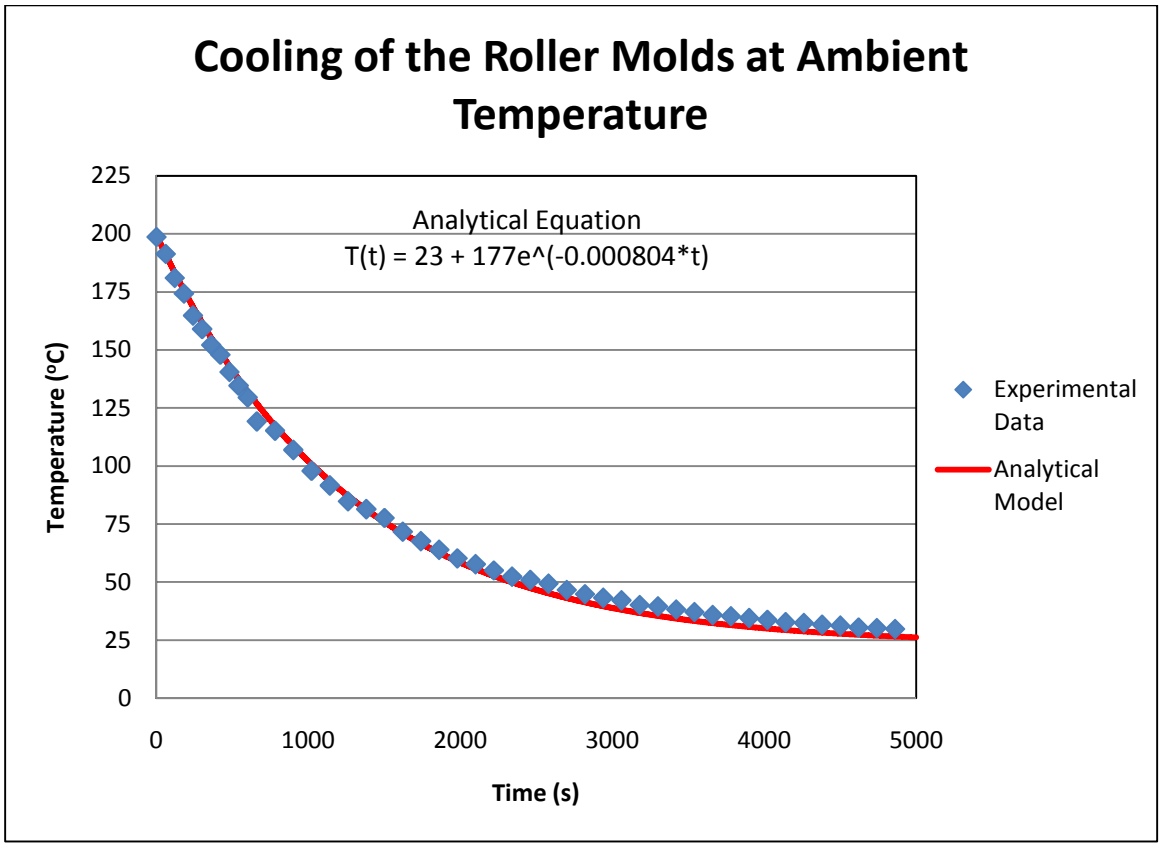

Figure 2-9 – Graph of experimental and theoretical cooling of rolls over time in ambient lab conditions.

Although oven heating of the rollers worked for trials of the machine, internal heating methods were researched for manufacturing considerations. The best option for heating the rolls in a manufacturing set up is to use medium temperature resistance heating tape as seen in Figure 2-10 [22]. These tapes are capable of heating the rollers to 260^{o} C while utilizing only 52 watts of power at 120 volts [22]. The temperature controller utilizes thermocouples to regulate the current (and thereby the temperature as well) of the tape. The only complicated element of the setup is allowing the rolls to rotate during while the tape is attached. To accomplish this, both the resistance tape and thermocouple would have to go through a slip ring for either roll. A slip ring is simply a

means of keeping electrical conductivity through a rotating assembly. For all the parts suggested here, the total price is less than $500 to internally heat the current version of the machine (see the machine budget in Appendix C).

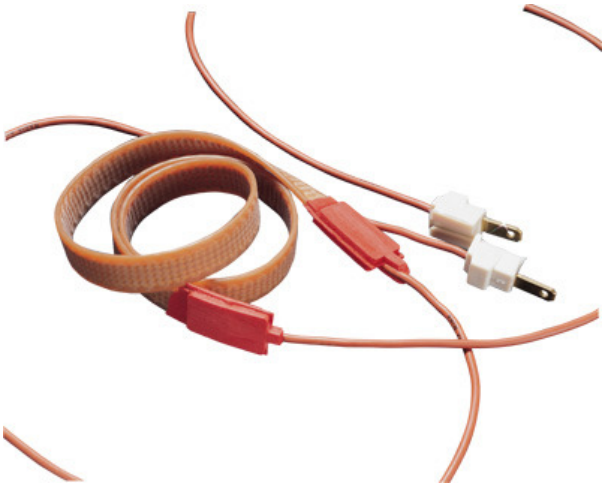

Figure 2-10 – Medium range resistance heating tapes. These are ideal for internally heating the rolls. The only caveat is that the wires must go through a slip ring to keep their electrical connection while the rolls are spinning. Adapted from [22].

2.6 Embedded Technology

One of the biggest advantages of this new process is the ability to embed a variety of materials within the microstructured PDMS during the continuous casting process. As can be seen in Figure 2-11, aluminum wire and a metal foil have each been embedded completely within the PDMS. Flexible embedding material is easier to use than stiff materials, however theoretically, not impossible. The material chosen for embedding must be able to withstand the heat of the process (typically 190^{o}C) and also cannot contain water, as the high heat causes water to vaporize and form bubble defects within the PDMS (Figure 2-12). These restrictions still leave a number of potential options to be

embedded with the microstructured PDMS created through this process, including flexible electronics and metal components.

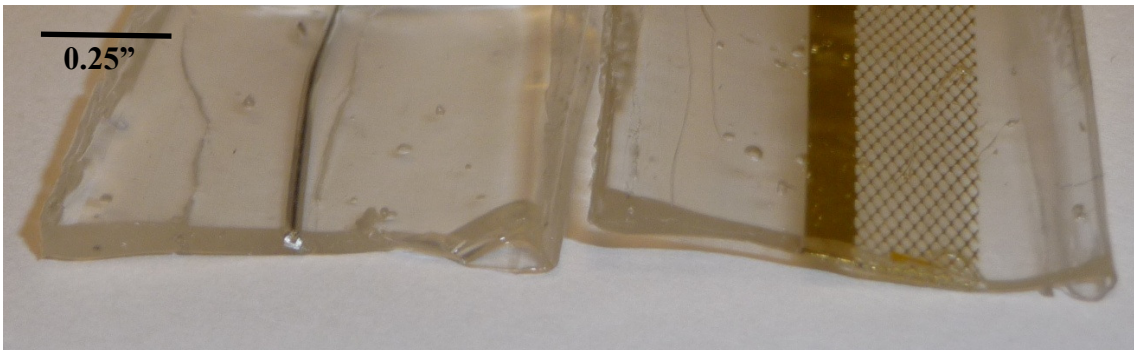

Figure 2-11 – Materials embedded within the PDMS. Metal wire (left) and foil (right) have been embedded within PDMS using the continuous PDMS casting process.

There are a number of potential applications for this embedding technology. Users can embed electronics in micro-electro-mechanical systems (MEMS) or microfluidic devices. It could also provide simple way to serialize parts as a unique serial number on foil can be embedded into each part, giving manufacturers a way to trace back possible issues to the point of creation of the device.

Figure 2-12 – Hazards of embedding improper materials. Embedding materials that can retain humidity, such as the paper demonstrated here, causes major defects as the heat of the process causes the water to vaporize while the PDMS is curing. Scale bar shown in the upper left is equal to 12 mm (~0.5").

2.7 Double Sided Patterning

Due to the fact that the machine uses two rollers to cure the top and bottom surface of the PDMS, the continuous casting fabrication method has the ability to create unique patterns on either or both sides. Figure 2-13 clearly shows that both surfaces of the PDMS have a micropatterned surface. Previously, to create a pattern on both top and bottom surfaces, one had to use soft lithography for two pieces and then bond them to each other back to back. This machine can now eliminate the bonding step altogether which is the most time intensive of the steps mentioned.

The ability to pattern both sides of a PDMS component could be useful in a number of applications. One application is to use the back side of the useful

microstructure for part numbering so as not to interfere with function on the device side. Although dealing with microstructures, the opposite side does could be on the macroscopic level for this identification. If the parts created were of a larger assembled system, this would allow assemblers down the line to accurately identify what part they are holding. Part numbering and part identification by assemblers is a major concern in not only accuracy of assemblies, but tracking parts through the process and inventory control.

Another possible use of this ability is to prepare the surface for an adhesive. Using current techniques, the side opposite of the desired pattern cures totally flat. While this ideal for temporary bonding, it is not advantageous when a bonding agent is to be used. The ideal surface for bonding is a rough surface that increases the amount of surface area the bonding agent covers.

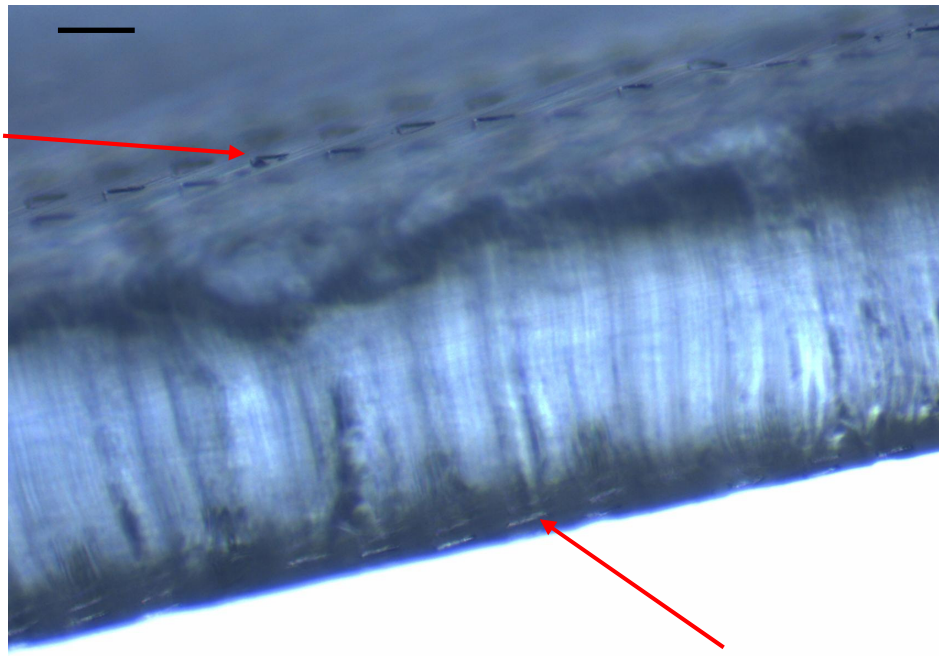

Figure 2-13 – Double sided patterning of PDMS. Optical microscopy image of PDMS on an angle that demonstrates patterning of both surfaces. Arrows indicate triangular features on each side. The scale bar shown in the upper left is equal to 120 µm.

CHAPTER 3 – WORKING PARAMETERS

3.1 Mass Flow Rate Balance

Defining a boundary volume for this process illustrates how the machine can be viewed from a thermodynamic point of view. Using thermodynamics to analyze manufacturing techniques is not new [23], but is useful in this situation to determine heat input needed based on the machine running conditions. Figure 3-1 shows the control volume for a steady-flow open system with an input of liquid PDMS prepolymer and an output of cured, micropatterned PDMS. The first step in this process is to balance the mass flow rate equation, given in Equation 3-1.

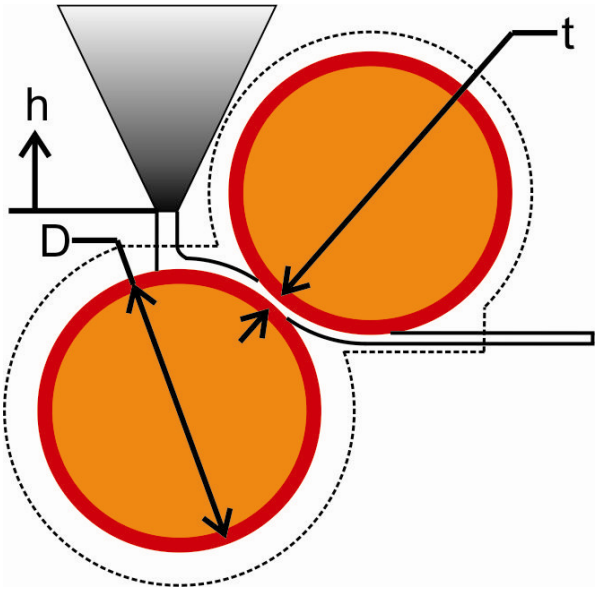

Figure 3-1 – Control volume of the process. The dotted line is the boundary of the control volume of the process when thought of in terms of thermodynamics. The inputs are work (turning the rolls), heat and liquid PDMS. The outputs are waste heat and cured PDMS.

$$\dot{m}_{in} = \dot{m}_{out} \tag{3-1}$$

From Equation 3-1, $\dot{m}_{in}$ and $\dot{m}_{out}$ (the mass flow rates into and out of the control volume, respectively) are related in Equation 3-2, where ΔP is the pressure of PDMS against the nozzle, R_h is hydrodynamic resistance of the orifice, ρ is the density of the PDMS, t is thickness of the final PDMS strip, w_{PDMS} is width of the final PDMS strip, D is diameter of the driven roller and $\dot{\theta}$ is the change in angle in rad/s of the driven roller.

$$\frac{\Delta P}{R_h} = \rho_{out} t w_{PDMS} \pi D \dot{\theta} \tag{3-2}$$

The liquid PDMS in this machine is gravity-fed and can be analyzed using equations relating hydrodynamic resistance to flow rate and hydrostatic pressure. Substituting in the relationship for hydrostatic pressure for ΔP in the previous equation gives Equation 3-3:

$$\frac{\rho_{in} g h_{PDMS}}{R_h} = \rho_{out} t w_{PDMS} \pi D \dot{\theta} \tag{3-3}$$

Here, g is gravity and h_{PDMS} is height of the PDMS above the nozzle. The hydrodynamic resistance of a round or rectangular opening is a function of the cross-sectional geometry, as seen in Equation 3-4:

$$R_h = \frac{8\mu L}{\pi R^4} \approx \frac{12\mu L}{w_{nozzle} h^3 \left(1 - 0.63\, {}^{h}/_{w_{nozzle}}\right)} \tag{3-4}$$

Here, μ is the kinematic viscosity of liquid PDMS prepolymer, L is the length of the nozzle (or the thickness of the acrylic plate in this case), R is the radius of the nozzle opening if round holes are used; w_{nozzle} and h are the width and height of a rectangular nozzle opening if rectangular holes are used. One important note with use of Equation 3-4 in regards to rectangular cross sections is that w_{nozzle} must always be smaller than h for this equation to be accurate.

Experiments were performed to determine the applicability of Equations 3-3 and 3-4 to the nozzle geometry used in this device. Experiments were run using the hopper setup used for the device, however, instead of letting the degassed PDMS flow onto the rollers, the hopper was placed over a cup on a scale. A set amount of PDMS was allowed to flow into the cup and timed. From this, mass flow rates and hydrodynamic resistance was calculated for each different set of openings. Figure 3-2 shows the experimental and theoretical hydrodynamic resistance values, which are in very good agreement. The parameters for this set of experiments were rectangular orifices of PMMA that were laser cut to the desired geometry. The column height for these experiments (h_{PDMS}) decreased as the experiment was performed, but the average was used for each individual trial. The most important fact to take away from this figure is that these values follow the curve almost exactly, albeit at slightly lower values. This set of experiments was also performed using circular orifices with similar results.

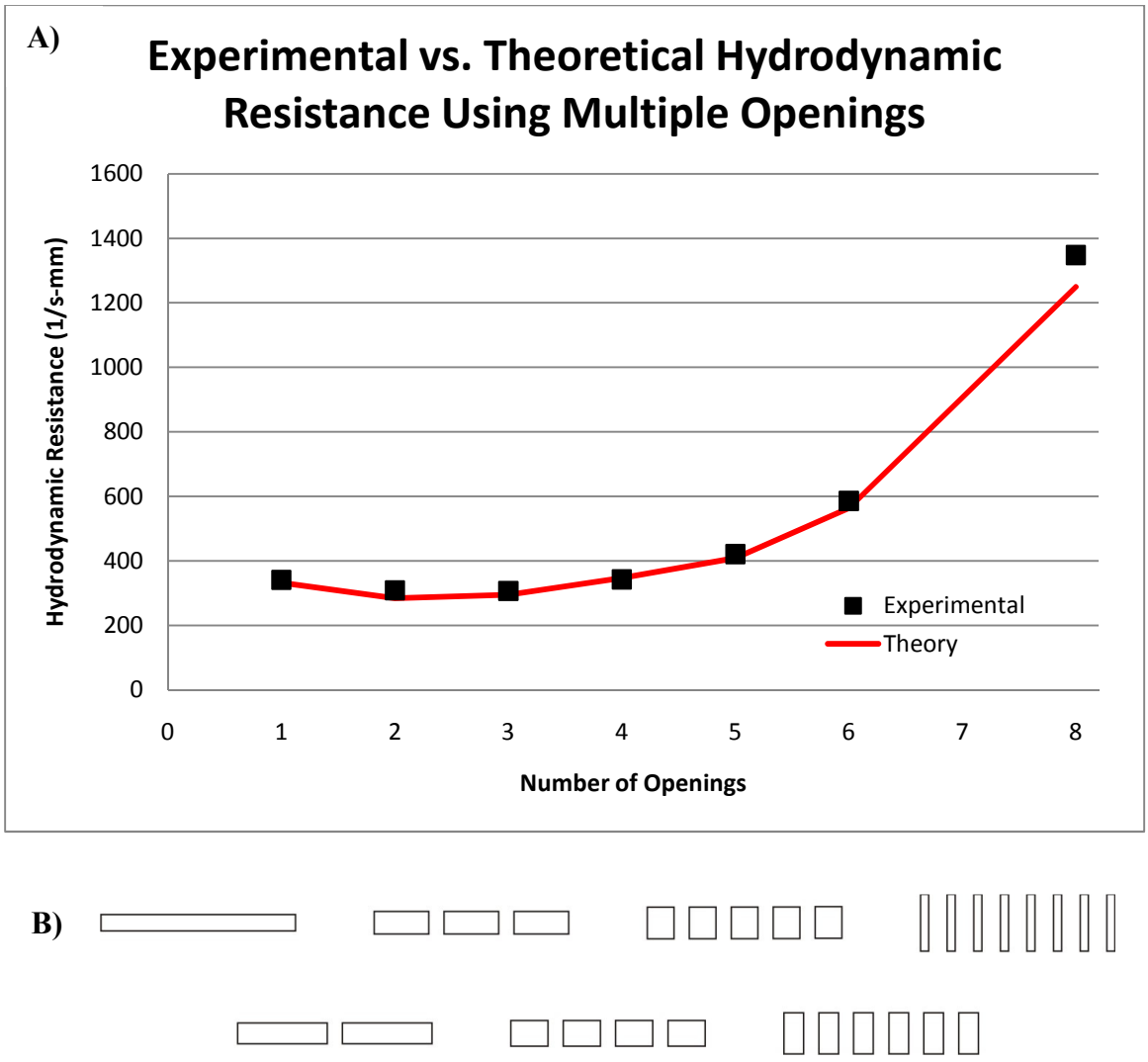

Figure 3-2 – Experimental verification of hydrodynamic resistance equations. A) Experimental and theoretical hydrodynamic resistance values for a number of nozzle geometries. B) Shapes of orifices used during the experiments. For dimensional information, please see Appendix D.

Although the ideal situation is to have a steady state system at work so Equation 3-1 can be calculated and put into use ahead of time, this is not always the case. Output of cured PDMS is regulated by the roller speed and any imbalance of the equation (i.e. too much or not enough liquid PDMS) would lead to overflow conditions on the roller or bad final product in the case of too little input. For a steady state to occur, the height of the PDMS above the orifice—and therefore the hydrostatic pressure used to drive the PDMS

feed—must be constant. However, since PDMS is flowing through the orifice, this height is constantly changing, while every other value is constant in Equation 3-1. Due to this, experiments run have used the average height throughout the run of the experiment for calculations and used as little PDMS as necessary to keep the variation in hydrostatic pressure small. Ideally, either the height would be kept constant or the roller speed would be regulated by the height of the remaining PDMS.

3.2 Roller Speeds

Although the machine cures PDMS in a seemingly simple manner, there are many interactions between the temperature, speed and PDMS input rate that all must work together to allow the machine to work correctly. Equation 3-1 describes the system if it is considered to be in steady-state. However, as stated earlier, with too much or too little input, results vary with a mess of uncured PDMS overflowing the system or bad product coming off the machine. While undercuring can be avoided in soft lithography by leaving the mold in the oven longer than necessary, in this system the roller speed and temperature must be carefully controlled to allow the PDMS to be fully cured on both sides when it leaves the machine.

One way to ensure complete curing of PDMS in the roller-casting system is to have a very low rotational speed of the rollers; the slower speed would allow the PDMS to remain in contact with the heated rollers for a longer period of time and absorb more thermal energy. However, since the goal of this system is to vastly decrease PDMS processing time, simply slowing the roller speed is not an ideal solution. In order to determine the ideal processing parameters, a number of tests were run to determine the

relationship between PDMS thickness, roller speed and temperature. Obviously, whatever changes in thickness and speed occurred had to be kept in check with the incoming flow rate according to Equation 3-1, but how these other variables interacted was unknown.

For the experimental data shown in Figure 3-3, it was decided to hold temperature constant at 190^{o}C. This temperature is the upper limit of this system because the PDMS used in these experiments (Sylgard 184) has a flash point between 214^{o}C and 250^{o}C, and a 10% margin of safety on that was to be maintained. There are two main reasons for only running the test at this temperature. One is that this temperature will allow the fastest speeds and make this system more advantageous to the user. The second is that the roller speed, thickness and temperature relationship creates a three dimensional graph and the easiest way to find these relationships is by holding two of the parameters constant.

Throughout the testing, it was noted that multiple different thicknesses could be attained at any one speed. This led to the finding that there is an upper and lower limit for attainable thicknesses at any one temperature and speed, which are shown in Figure 3-3. From this data, a couple of facts jump out. The first is the confirmation of the initial theory that decreasing the thickness of the fabricated PDMS will enable faster roller speeds. Interesting though is the fact that the lower limit is very stable and roller speeds need to increase dramatically for thicknesses of less than roughly 0.25 mm. The reason for this phenomenon is not known, however, the author does provide the theory that it is a result of the viscosity and spreading characteristics of the PDMS itself which causes the PDMS to cure before reaching the second roller.

Some other interesting notes from the graph are also how well logarithmic functions fit the data. Although a squared function fits the data slightly better, the minimum thickness of the square function for the lower limit is roughly 17 rpm. This suggested that lower thicknesses could be achieved at lower speeds, which is not true. A logarithmic function became the better option due to this fact and because at a roller speed of 0 rpm, a theoretically infinite thickness of PDMS can be cured. Obviously as the speed approaches 0, the thickness will approach infinity.

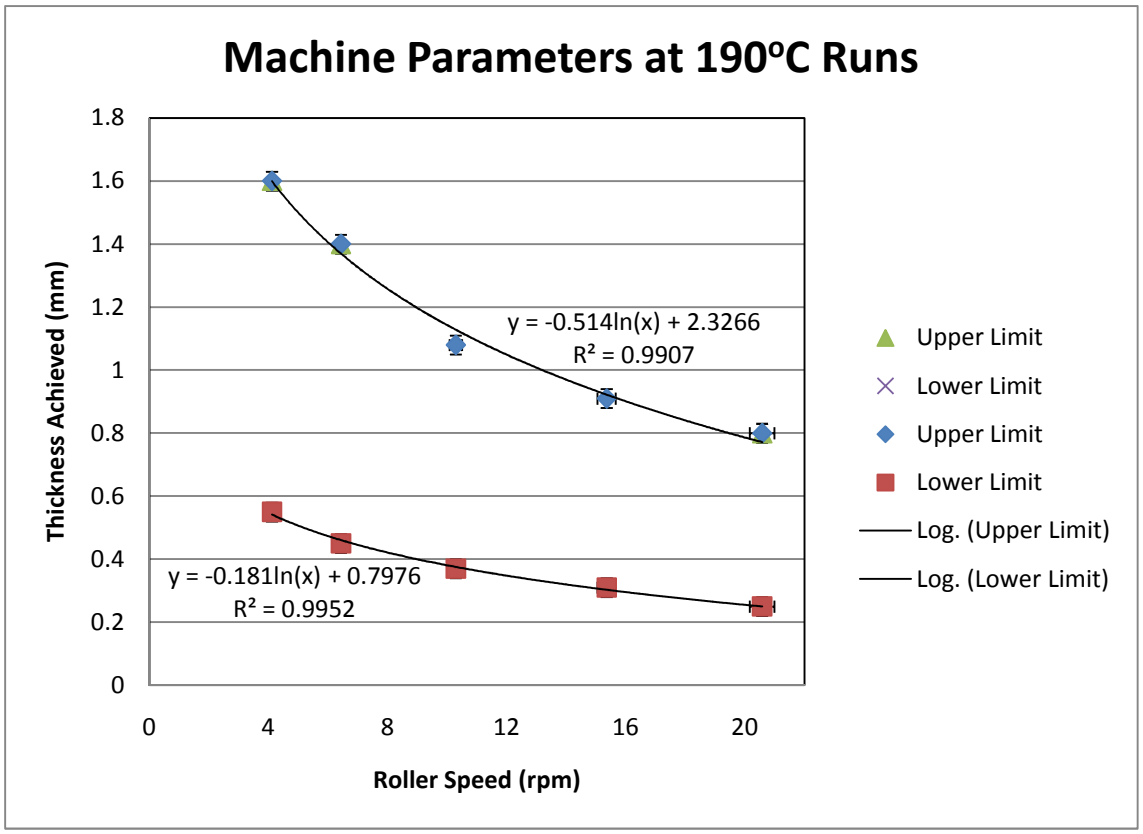

Figure 3-3 – Machine parameters. Upper and lower limits of operating parameters for the continuous-casting machine at 190°C are labeled.

Another interesting observation is that the operating window of the system becomes smaller with an increase in roller speed. This is proposed to be due to the fact that at lower speeds, an over-curing can occur. This means that the PDMS is on the rollers longer than it needs to be for curing. This does not affect the final product in any way as this is what happens all the time during soft lithography. The product is left under heat well after curing takes place. This margin of error however becomes smaller with faster roller speeds making the working parameters of the machine smaller.

Although the upper and lower limit regression equations found for these data points will never technically meet, these equations may not be valid for larger roller speeds. The maximum speed for this system will likely be limited by the mechanical properties of PDMS. There is a thickness threshold under which the PDMS tends to break inconsistently and become extremely difficult to handle. This is due to a number of reasons and their interactions with one another. The primary reason is that the peeling force to removed the cured PDMS from the rolls is constant (~0.15 N/mm line contact strength; details of this calculation can be found in Appendix E) and as the thickness of the material decreases, the stress increases and the PDMS breaks.

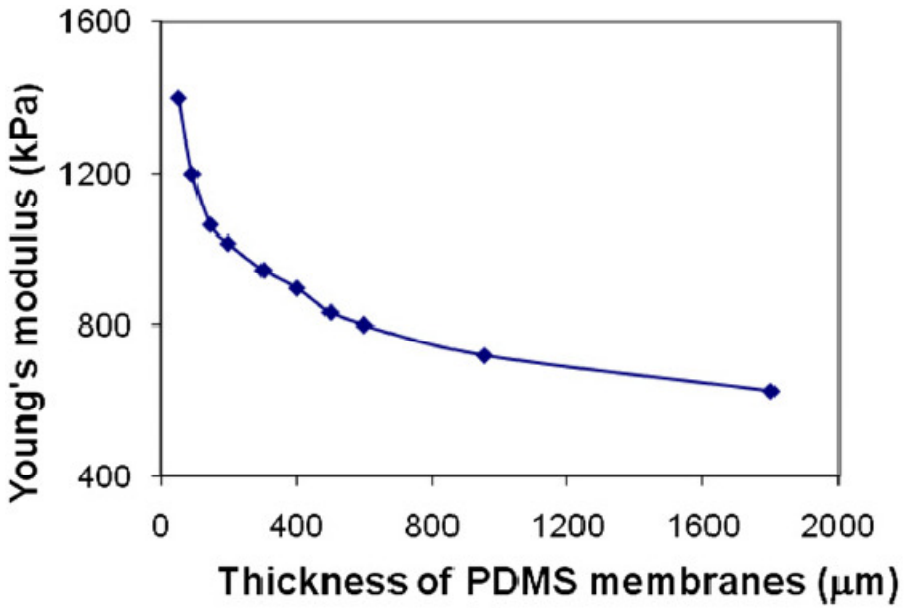

Figure 3-4 – Thickness of PDMS membrane vs. Young's modulus. As the thickness of PDMS decreases, Young's Modulus increases exponentially. Adapted from [24].

Another reason the PDMS becomes difficult to handle at small thicknesses is due to the fact that the mechanical properties of PDMS are thickness dependent [24]. As seen in Figure 3-4, as the thickness of PDMS gets smaller, Young's modulus increases exponentially. This means that the PDMS becomes stiffer and requires more force to deform. PDMS also has an extremely high coefficient of static friction against steel (μ = 1.46). The less the material deforms, means higher normal forces against the sidewalls of the rolls and translates to higher forces needed to remove the material from the rolls, causing stress to go above what the material can handle. The final reason proposed here is due to the geometry of the system itself. The current setup, as stated earlier, uses rollers not specifically designed for this purpose. The rolls have chamfers on the edges, as seen in Figure 3-5, that add thickness to that small section of the PDMS that cure against this area. In addition to this added thickness to the sides of the film created, this unique

geometry on the walled roller adds to the amount of peeling force needed to remove the film from this roller.

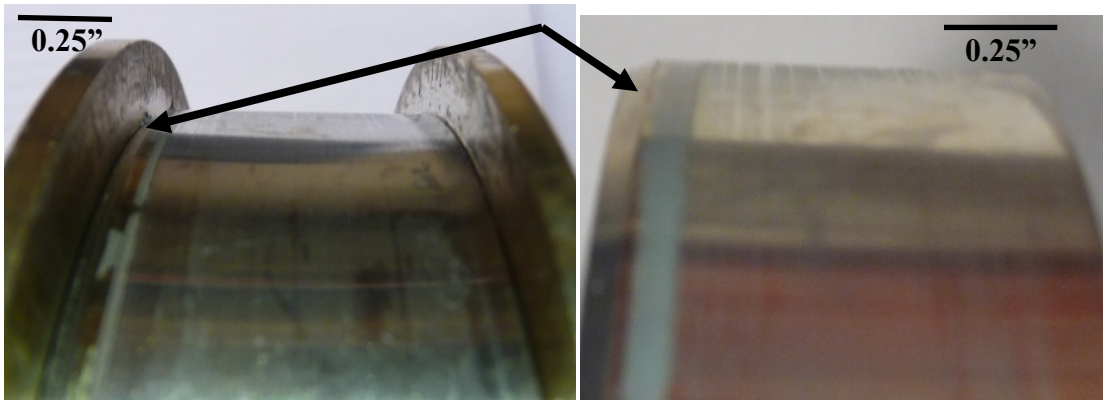

Figure 3-5 – Rollers used for the machine. Originally designed as bearings, the rollers have chamfers at one of their edges. This chamfer causes issues for thin sheets by increasing the amount of force needed to debond the PDMS from the walled roller (left). This is one of the reasons the working limit on the thickness that can be created is 0.15 mm.

If the upper bound shown in Figure 3-3 continues at higher roller speeds, the minimum workable thickness for this system is predicted to be roughly 0.15 mm. Below this thickness, the delaminating force from the rollers tends to crack or break the films created. This threshold will reach the lower limit at roughly 34 rpm of roller speed and the upper limit at about 75 rpm. These numbers correspond to an operating temperature of 190^{o}C.

3.3 Energy Balance

Another important detail about the system is how much energy is actually needed to run the system. As seen in Figure 3-1, the system can be modeled as a constant volume thermodynamic problem as could any manufacturing process [23]. With some minor

assumptions, one can see through the following derivation how much energy would be needed to maintain constant roller temperature during steady state operation. The calculations begin with applying conservation of energy for a control volume at steady state:

$$\dot{E}_{in} = \dot{E}_{out} \tag{3-5}$$

Within this system, heat is transferred from the rolls to the PDMS for the curing process and work is also input to turn the rolls and move the PDMS. Equation 3-5 is evaluated using these parameters in Equation 3-6 where $\dot{Q}$ is heat transfer, $\dot{W}$ is work done and $\dot{H}$ is enthalpy transfer:

$$\dot{Q}_{in,heat} + \dot{W}_{in,motor} + \dot{H}_{mat,in} = \dot{W}_{out} + \dot{Q}_{out} + \dot{H}_{mat,out} \tag{3-6}$$

In the case of this system, energy enters in the form of heating of the rollers, work provided by the motor to turn the rollers and enthalpy of the PDMS at room temperature. Energy leaves the system as work done moving the PDMS, heat leaving the rollers into the surroundings and enthalpy of the cured PDMS leaving the system. Rearranging Equation 3-6 produces Equation 3-7 to show what is actually needed as far as system inputs. Notice that work is removed from the equation due to its relative insignificance when compared to the other terms.

$$\dot{Q}_{in} = \dot{Q}_{out} + \dot{H}_{mat,out} - \dot{H}_{mat,in} \tag{3-7}$$

The heat out term can be broken down into the two components, accounting for radiant and convective heat losses. The enthalpies of the material are equal the mass flow rate times the specific heat of the material times the temperature at each state. Substituting these values into Equation 3-7 yields Equation 3-8:

$$\dot{Q}_{in,heat} = (h_{conv} + h_{rad})A\Delta T + (\dot{m}cT)_{out} - (\dot{m}cT)_{in} \quad (3\text{-}8)$$

Here, h_{conv} and h_{rad} are the convection and radiation heat transfer coefficients (respectively), A is the surface area of the roller exposed to heating losses, ΔT is the temperature difference between the roller and the surrounding environment, $\dot{m}$ is the mass flow rate, c is the heat capacitance of PDMS and T is the temperature of the PDMS. The exposed area of rolls to heat loss is 89.663 in^2 or 0.0578 m^2. The values for the heat transfer coefficients in this case are 7.45 W/m^2K for convection and 2.44 W/m^2K for radiation. Details on the calculation of these values can be found in Appendices A and D respectively.

While it is difficult to find values for the specific heat of the proprietary PDMS material used in this study (Sylgard 184, Dow Chemical), it can be estimated using data from [25] on a PDMS monomer. For PDMS monomers, the heat capacitance is 117.775 J/molK while the molar mass is 74.1539 g/mol. From the manufacturer's product specification data, the density of Sylgard 184 is 1027 kg/m^3 [18]. During steady state operation of the machine, there is assumed to be no wasting of material and mass flow into and out of the system is constant at a rate determined by Equation 3-9 where t is the final thickness of PDMS and w_{PDMS} is the final width.

$$\dot{m}_{in} = \dot{m}_{out} = w_{PDMS} t \omega R \rho_{solid}$$

$$\dot{m}_{in} = \dot{m}_{out} = 0.0254m * t * \omega * 0.1397m * 1027\,{}^{kg}/_{m^3} \tag{3-9}$$

$$\dot{m}_{in} = \dot{m}_{out} = 3.644 t\omega\,{}^{kg}/_{s}$$

Plugging the above into Equation 3-8 leaves Equation 3-10 as the final equation representing the amount of power needed from the internal heaters to keep the system constantly running at 200°C

$$\dot{Q}_{in,heat} = \left(7.45\,{}^{W}/_{m^2K} + 2.44\,{}^{W}/_{m^2K}\right)(0.0578m^2)(177\text{K})$$
$$+3.644t\omega\,{}^{kg}/_{s}\left(117.775\,{}^{J}/_{molK}\right)\left(\frac{1000\,{}^{g}/_{kg}}{74.1539\,{}^{g}/_{mol}}\right)(473K - 296K) \tag{3-10}$$

$$\dot{Q}_{in,heat} = [101.181 + 1.0244 * 10^6 * t\omega]W$$

Obviously thickness and speed of the rollers play a large role in this equation, however, as seen in Section 3.2, the typical values of these numbers are very small. Using the parameters of the system found in Figure 3-3, thickness will fall between 0.0002m and 0.002m while ω ranges between 0.4 rad/s and 2 rad/s.

CHAPTER 4 – DEFECT CHARACTERIZATION

4.1 Defects Observed, Causes and Solutions

Although defects is never a term one wants in a process, especially in a manufacturing sense, they do occur and it is important to recognize their causes and how to reduce the amount of defects seen in the process. For this system, there were only two types of recurring defects observed during testing. Figure 4-1 shows both types of defects which can be broken down into two major categories: surface defects and subsurface defects. Although subsurface defects when dealing with microstructures on the surface may seem like a minor issue, if these defects become too frequent and/or large, they will interfere with surface characteristics. For this reason, when users observe these types of defects, they should proactively take the steps outlined here to reduce and/or eliminate them.

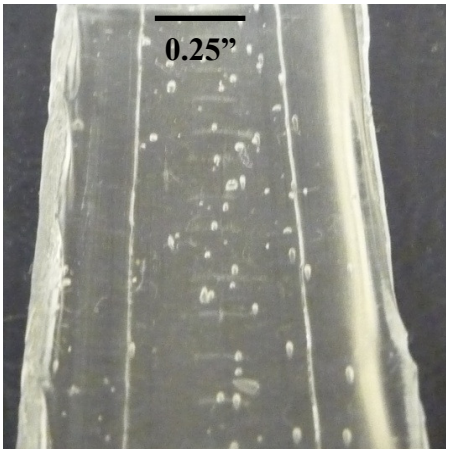

Figure 4-1 – Surface and subsurface defects. The faint lines that are running parallel to the edge are surface defects while the small air bubbles in the middle of the sheet are within the PDMS and below the surface.

4.1.1 Surface Defects

As with any new process, there are bound to be small functional issues that must be resolved. For this process which accurately replicates microstructures on the surface of PDMS, the formation of unwanted defects on the surface is a major concern. These defect types were observed in early experiments with the machine, and were caused by the way that liquid PDMS is transferred onto the rollers. As can be seen in Figure 4-2, PDMS initially stays in a small center area of the first roller when using a single rectangular orifice. As the PDMS comes into contact with the second roller, the PDMS spreads to cover the entire width of both rollers. After curing however, there are noticeable lines in the PDMS that are in the same areas where the edge of the liquid PDMS stopped before coming into contact with the second roller. These lines, as seen in a cross sectional view in Figure 4-3, are crevices on the surface.

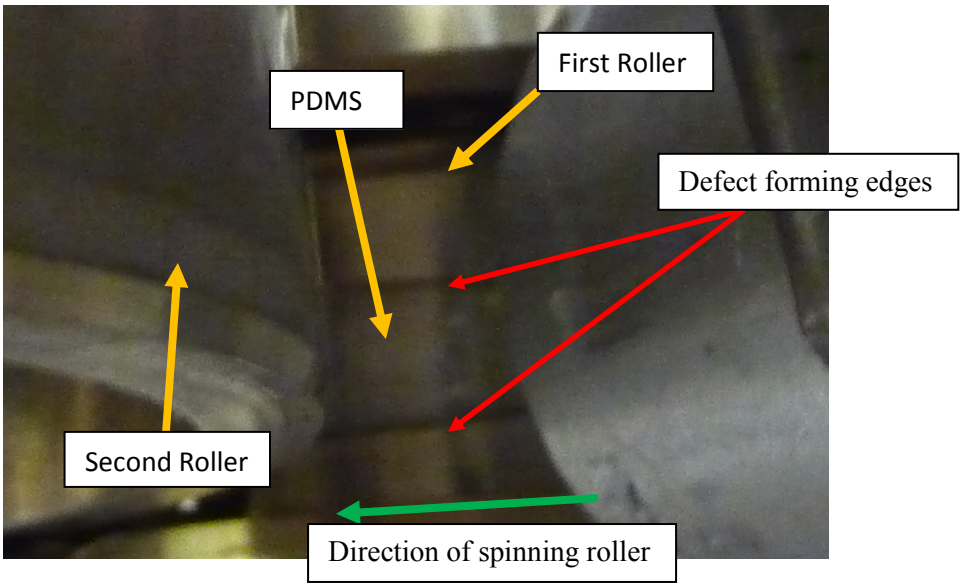

Figure 4-2 – Machine as surface defects are forming. As PDMS flows through the orifice onto the first roll, the stream stays centered below the orifice until it comes into contact with the second roller that forces the PDMS to spread to the width of

both rollers. If the PDMS is applied unevenly to the first roller, it can result in surface defects.

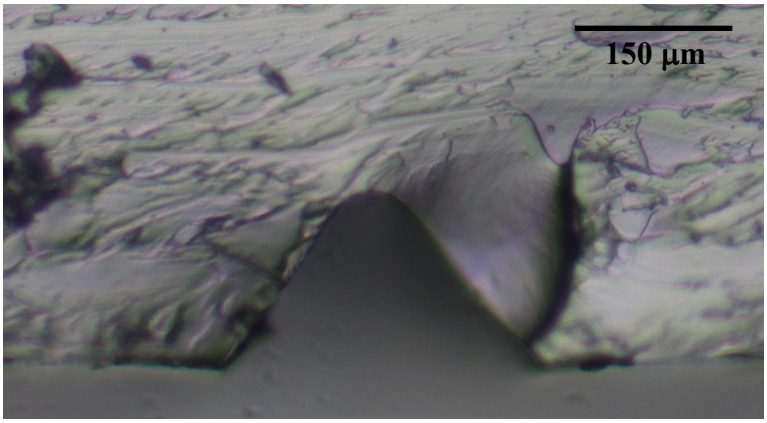

Figure 4-3 – Optical microscopy image of a cross section of a surface defect. Seen from above or below, these defects appear as lines running parallel to the edges; these crevices can run the entire length of the sheet produced and can be as large as 300 µm across and 400 µm deep.

The problem is that a small layer of PDMS is curing on the first roller before being spread to the entire width by the second roller. Figure 4-4 shows how these defects occur: a thin layer of cured PDMS forms a barrier that does not allow the liquid PDMS to flow properly to all portions of the mold. Although the PDMS is only in contact with the bottom roller when the problem starts (Figure 4-4a), the entire area is extremely hot and the PDMS is being cured on the sides that are technically not in contact with either of the rollers. As the PDMS is forced to cover the entire roller, this time by the force of the second roller, this same leading edge occurs. Although at long flow times liquid PDMS will flow to cover all areas of our mold, the process is designed to speed the curing of the PDMS. The short flow times of our machine do not allow the quickly curing PDMS to squeeze under the already cured layer. It simply flows past it to the path of least

resistance. What are left after this occurs are the surface defects that appear as lines in the finished product.

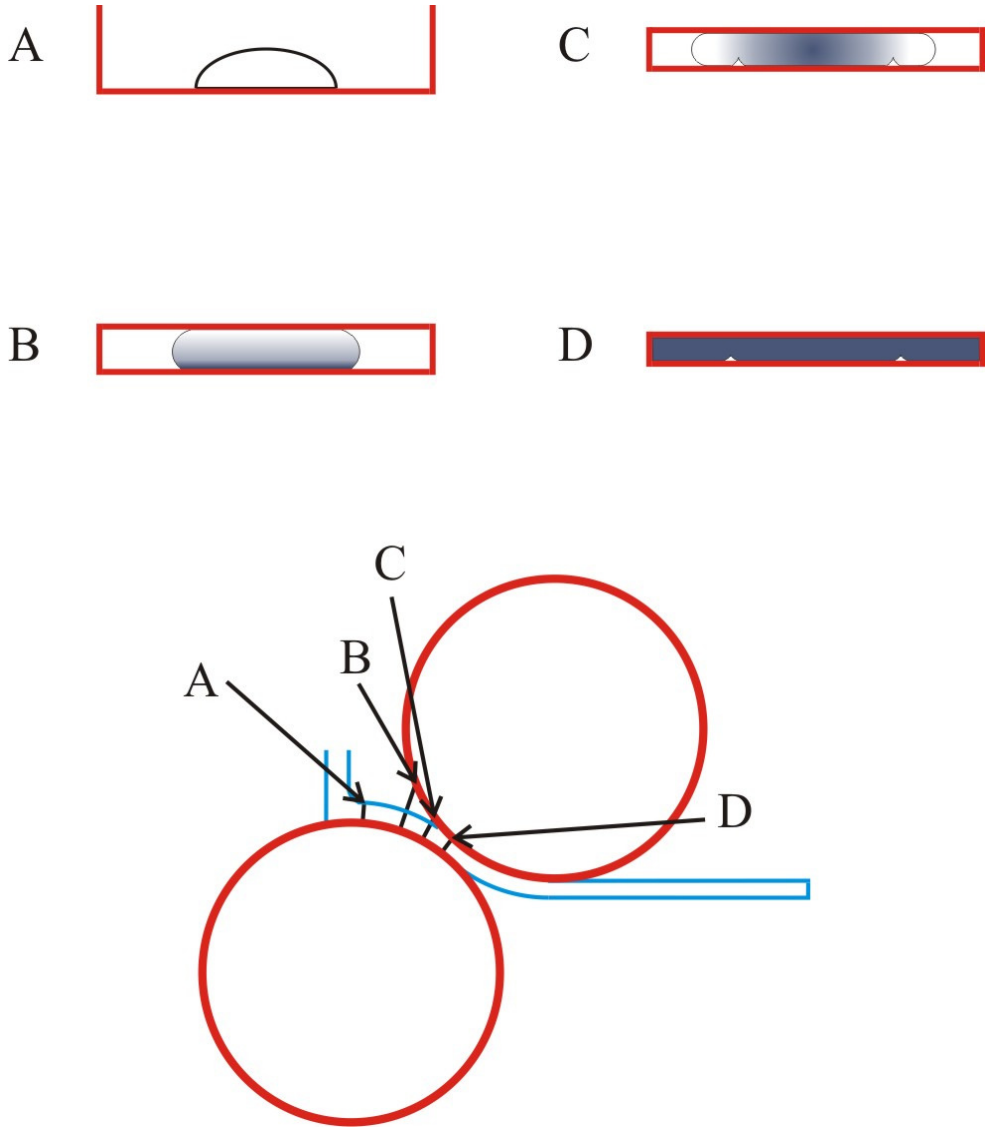

Figure 4-4 – Diagram of how a surface defect form. A) Liquid PDMS initially falls in a stream onto the middle of the first roller. B) As it reaches the second roller, the uncured PDMS is forced to spread out to cover the roller surface; however, the PDMS in contact with the first roller has already cured. C) PDMS is forced to flow over the already cured portion, but it does not flow back under. D) The PDMS is now fully cured with surface defects.

Figure 4-5 shows an edge similar to one that causes the initial formation of a surface defect in the PDMS continuous casting machine. This experiment was performed on a hot plate and shows how the PDMS cures on the bottom face while it is being squeezed by a top plate, simulating the second roller in the machine. It is noticeable that the leading edge has a contact angle that is larger than 90^{o}. Despite the complexity of the issue, two simple solutions have been found to eliminate these types of surface defects in PDMS.

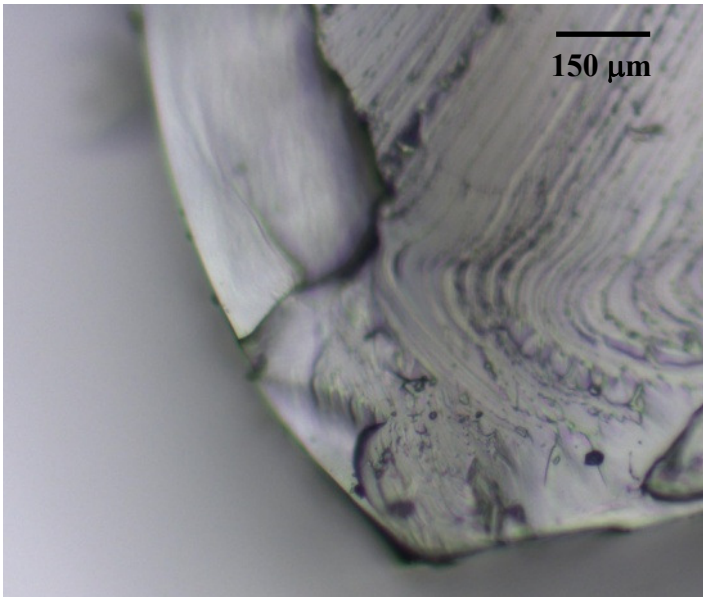

Figure 4-5 – PDMS surface defect caused by parallel plates. A parallel plate was used to simulate the force of the second roller forcing the PDMS to cover the entire width of the roller. The large contact angle on the leading edge (left hand side) obstructs uncured PDMS from filling out the entire mold, causing surface defects to occur.

One way to prevent this type of surface defect is to design a nozzle that forces the PDMS to fall in a sheet that covers the entire width of the roller. However, making an extremely viscous liquid fall in a uniform sheet can be challenging. In order to test

different nozzle geometries, multiple nozzles were designed that had different numbers of openings but all had the same total hydrodynamic resistance. Using the equations from section 3.1, it is possible to calculate the resistance of an individual opening; for these nozzles, the resistance value has to remain the same for multiple openings which are now in parallel. Similar to electrical resistance, the hydrodynamic resistance of openings in parallel can be calculated by taking the inverse of the sum of the inverses, as shown in Equation 4-1.

$$R_{total} = \left(\frac{1}{R_1} + \frac{1}{R_2}\right)^{-1} \tag{4-1}$$

When first implementing the use of the gravity-fed PDMS reservoir, a nozzle with a single rectangular opening the width of the roller was used. However, despite the width, the liquid PDMS always flowed into the center of the roller and caused the defects. After this occurred, the thought was to use multiple openings to dispense the PDMS evenly over the roller. This reduced the problem, however, placement and spacing between the openings was critical and using the current setup the total surface area available for the nozzle was limited. This led to the use of circular openings because circular orifices have a lower resistance per unit of area than rectangular orifices. This allows smaller circles and total surface area to be used for the orifice. After many attempts with different placements, it was found that an overlapping pattern, as seen in Figure 4-6, was the optimal solution for this setup. Using this type of nozzle geometry completely eliminates surface defects, as shown in Figure 4-7.

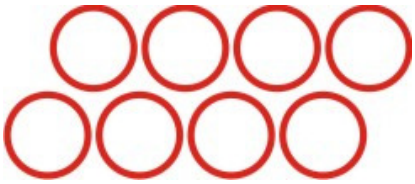

Figure 4-6 – Pattern of orifices to eliminate surface defects. This typical pattern of overlapping circles is used to eliminate defects in the final product. Actual sizes of the circles will depend on the needed hydrodynamic resistance for based on the parameters of the machine trial.

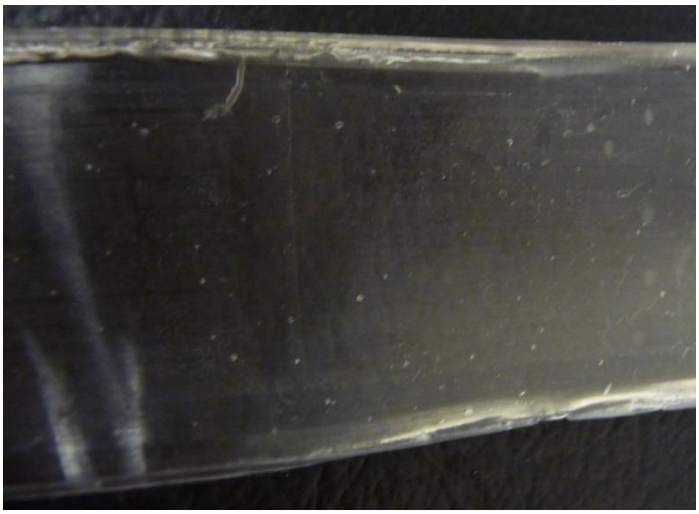

Figure 4-7 – PDMS without surface defects. This is PDMS created after adjusting the type and geometry of nozzles, eliminating surface defects.

The distance between the circles in the nozzle is of critical importance. If the openings are spaced too far away from one another, then multiple sets of the original defects are created. A number of these types of defects are shown in Figure 4-8; all were caused by improper separation of the openings. Conversely, if the orifices are too close to one another, the liquid PDMS will flow around the separating feature and appear as if it flowed through a single orifice causing surface defects. This phenomenon is shown in

Figure 4-9; here both nozzles have four openings, but with different spacing. The orifices need to be as close together as possible to create even coverage on the roller, however, the streams cannot run together. The experiments performed as part of this thesis indicate that the edges of the orifices can be as close as 0.05" apart and still have separate streams. Therefore it is recommended to keep the openings at 0.05" apart for the best coverage of the rolls and thereby elimination of the surface defects.

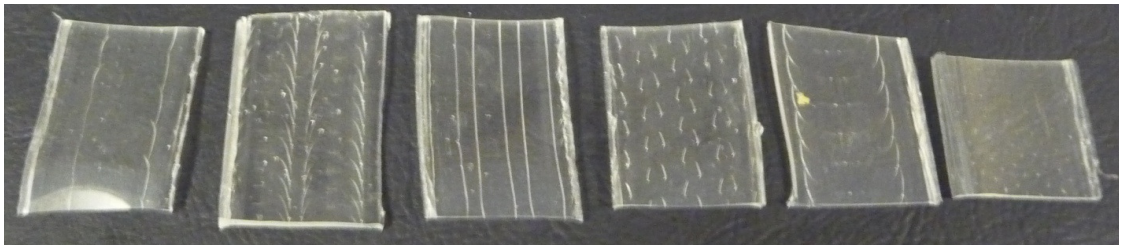

Figure 4-8 – Defects caused by improper nozzle geometry; openings were spaced too far apart, causing multiple sets of surface defects. From left to right, PDMS was produced with 1 through 6 openings and surface defects are still apparent.

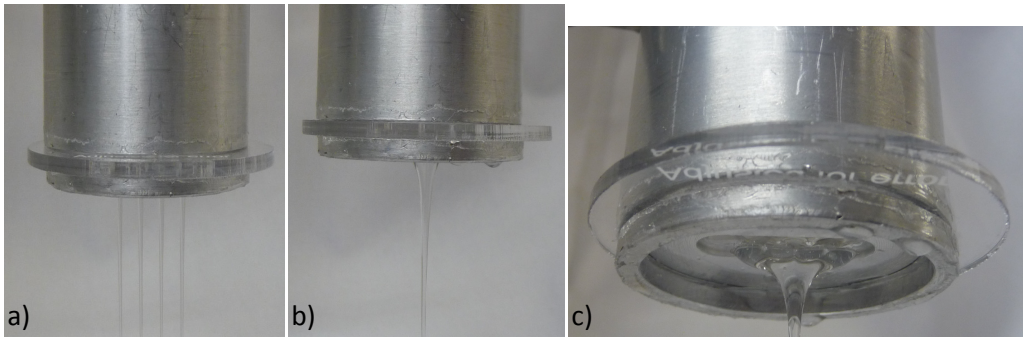

Figure 4-9 – Effect of poor nozzle spacing. The spacing between the openings is critical. In each of these images four openings are used, however in (a) the openings are properly spaced with edges 0.05" apart. In (b) and (c) the edges are too close to one another and the liquid PDMS forms a single stream.

Another way to avoid surface defects is to reduce the operating temperature of the system. Because surface defects are caused by PDMS is curing before spreading along the entire width of the roller, lowering the temperature gives the individual PDMS time to fully coat the roller before curing, thus reducing the chance of defects occuring. As seen in Figure 4-10, lowering the temperature from 190^{o}C to 160^{o}C reduces the significance of the defects using one rectangular orifice. When the temperature of the system is reduced further to 125^{o}C, the defects completely disappear. Although this method is a viable means of eliminating surface defects, reducing the operating temperature necessitates a corresponding decrease in roller speed. Since the major advantage of this system over soft lithography is its low processing time, using a method of eliminating defects that also reduces throughput is nonideal. This method is therefore considered a secondary option compared to selecting the proper nozzle geometry, as previously described.

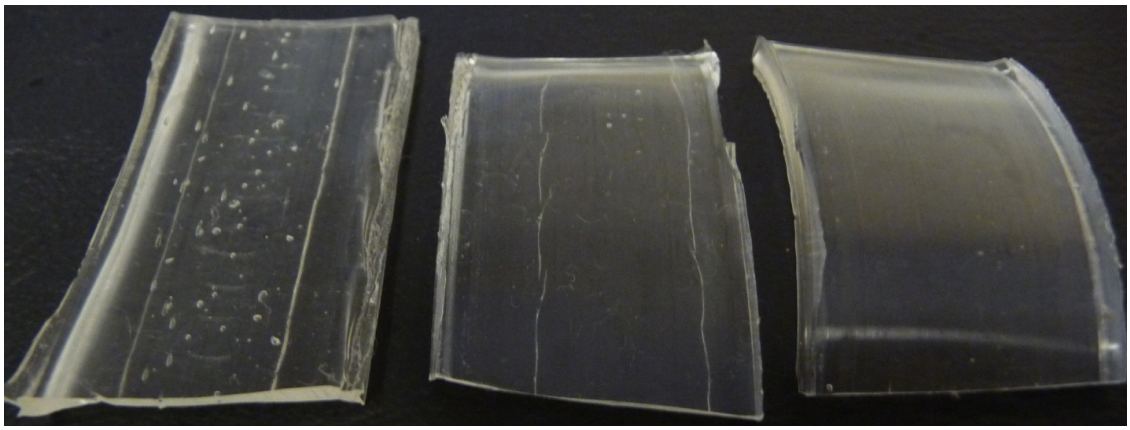

Figure 4-10 – Effects of temperature of surface defects. PDMS created at different operating temperatures in order to eliminate surface defects. From left to right, the machine was run at 190^{o}C, 160^{o}C and 125^{o}C. The surface defects are noticeably smaller at 160^{o}C when compared to 190^{o}C and eliminated in the 125^{o}C trial.

4.1.2 Subsurface Defects

Although for most applications subsurface defects are not as catastrophic as surface defects, they may still damage the quality of the final product. There are two major causes of surface defects. The first only occurs when embedding certain materials within the PDMS; any material that contains water, however miniscule will cause subsurface defects as the temperature of the machine causes the water to boil out during PDMS curing (Figure 2-10). Materials like paper absorb some amount of water from the humidity in the environment, when the paper and PDMS are heated, the water vapor bubbles it way through the liquid PDMS prepolymer as it is curing and causes defects throughout the material. This problem can be avoided by carefully monitoring the materials that are being embedded with the PDMS.

The other major cause of subsurface defects is from air bubbles trapped within the PDMS as it cures. The normal mixing process of the two PDMS prepolymer components causes a large volume of air to become trapped in the viscous liquid. This is a common occurance with PDMS and is normally dealt with by degassing the liquid PDMS prepolymer in a vacuum chamber; however sonication or placing the liquid prepolymer in a centrifuge have also been shown to accomplish the same task. During machine runs the PDMS was degassed in a cup and then poured into the funnel with the nozzle which dispensed the PDMS onto the rollers. It was this pouring step that had caused many of the air bubbles to be reintroduced in the prepolymer. By forgoing this step and vacuum degassing in the funnel itself with the orifices closed off, it eliminated the subsurface air bubbles in the final product.

CHAPTER 5 – ROLLER FABRICATION

5.1 Material Removal Fabrication Techniques

With any device, the manufacturability of components is a primary concern for it to be considered a viable product. Although most of this machine can be easily made in a typical machine shop, the rolls are one thing that cannot. Because PDMS that is created using this process will have identical surface features as those seen on the roller molds, they are the most critical part of the machine. As seen in the budget, they are also the most expensive part as well: costing up to almost $10,000 per roll, depending on the pattern desired.

This section will cover roll fabrication techniques that remove material from what is termed a virgin roll. A virgin roll has the final machine dimensions and a precision ground outside surface that is less than 20 microinches on the Ra scale. This means that the average deviation from the mean surface must be less than 20 microinches [26]. After the virgin rolls are processed using one or more of these techniques, it is considered a complete roller mold and is ready to be used within the machine. The costs of the processes described in this section are dependent on the number of features desired in the roll. These processes are also considered to be the more durable than material addition processes due to the fact that the features are cut into the stainless steel of the roll itself.

5.1.1 Micro-Milling

Although micro-milling is typically used to create very small parts for watches and surgery, this process could be used to modify the surfaces of virgin rolls to produce the rollers needed for this system. Micro-milling is a process very similar to conventional

milling, however, it employs tools that can have a diameter of less than 50 um [27], as seen in Figure 5-1. To achieve acceptable material removal rates, the ratio of the feed rate per tooth to the tooth radius must be increased. This causes high stress on the tool itself, which leads to more tool breakage that cannot always be seen by the human eye [28]. This dramatically increases the expense of the process as broken tools may affect the surface of the part, in this case the roll. However, with surface roughness capabilities of up to 0.3 μm [29] on the Ra scale and features capabilities down to 25 μm [27], this technique is practical for the intent of this project.

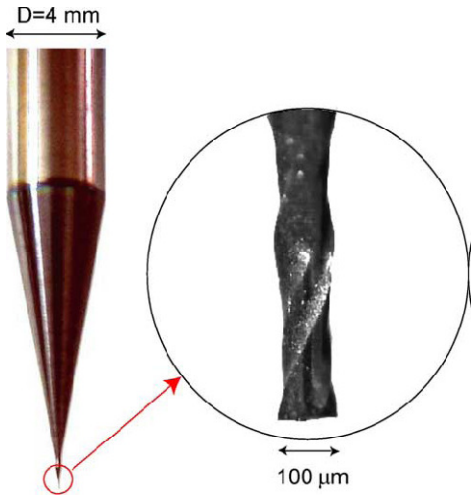

Figure 5-1 – Example of a tool used in micro-milling. Although the chucking area is 4 mm in diameter, the double fluted endmill is only 100 μm in diameter. Adapted from [27].

5.1.2 Micro-Electrical Discharge Machining

Electrical discharge machining uses tools that emit a controlled spark that erodes the workpiece into the desired shape—as opposed to using conventional machining tools that make contact with the workpiece. With this controlled spark three dimensional

shapes can be created with multi-axis motion machines [30], similar to traditional machining. This method of machining can produce feature sizes as small as 20 μm with aspect ratios of 10 and surface roughness of 0.2 μm on the Ra scale [31]. Figure 5-2 is an example of a part created by the EDM process displaying a very high aspect ratio. This may be desirable for producing the rolls depending on the type of features desired. However, as with micro-milling, tool life and cost is a major issue. As the tool sparks and erodes the workpiece material, the tool also erodes, albeit at a slower rate. This means that to remove a lot of material, such as that needed to create the large surface area rolls in this work, cost will to be extremely high. Estimates for a simple design, seen in Appendix F, range from $4,000 - $9,000 per roll.

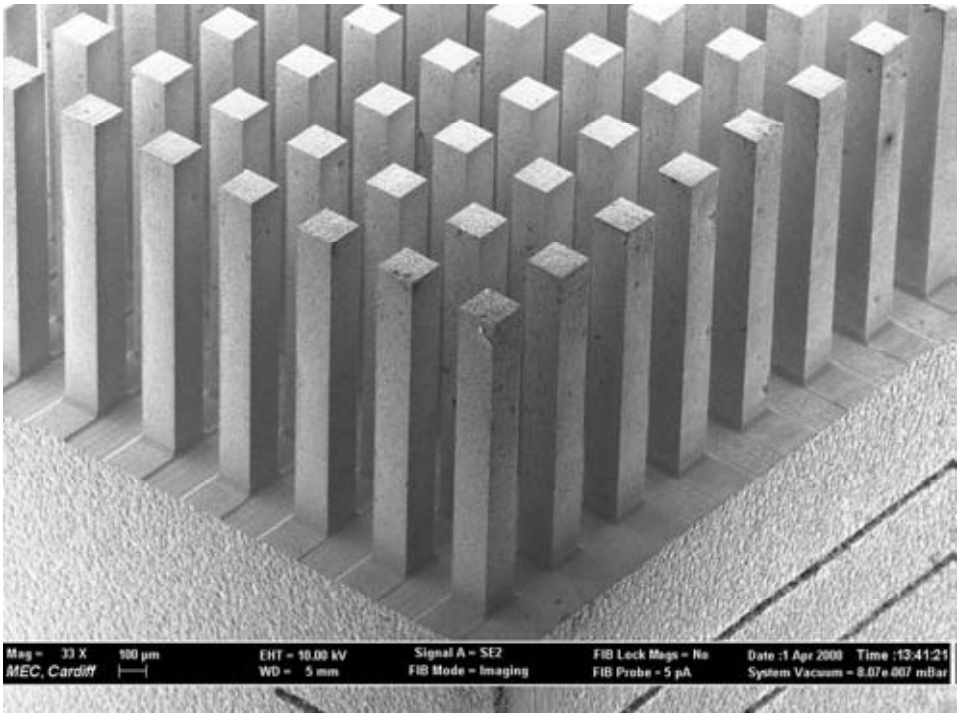

Figure 5-2 – EDM capabilities. This is an example of a part made using the EDM demonstrating the high aspect ratio capabilities of this process. Adapted from [30].

5.1.3 Laser Welding and Milling

Laser milling uses a high-powered laser to remove material from a workpiece. Ideally, all the energy released by the laser would be absorbed by the workpiece and vaporize the material. However, the laser can be reflected and transmitted as well, which leads to losses in the system of up to 80% [32]. This is a non-contact process and unlike the micro-EDM process, no specialized tools need to be created for each part; instead the laser is guided directly from a 3-D CAD model. The downside is the long machining time and the possibility for creating heat affected zones, or HAZs. The long machining times will lead to increased costs, but the HAZ can be mitigated by using extremely short pulsed lasers [33]. For the purposes of creating the rolls needed for this process, it is recommended that and Excimer laser be used. Using laser ablation techniques, feature sizes as small as 5 μm have been claimed [34] as well as surface roughness as low as 0.8 μm Ra [35].

An Excimer laser—the type selected for this process—is one of the most widely used laser types in industry. It is a pulsed laser with a fast electrical discharge in a high pressure mix of a rare gas and employs a halogen gas for light emission. This type of laser is typically used in extremely small pulses (10-100 ns) making it extremely well suited for micromachining applications due to the fact that fast pulsed lasers can remove material smaller than the spot size of the beam [33]. This occurs due to the Gaussian distribution of energy within the beam with the highest point being the center of the beam. Features as small as 1/10 the size of the beam have been created by adjusting the beam intensity so that only the center of the beam is above the threshold for a given material [33].

Although this section is focusing on material removal technologies, using laser techniques could also add material [36]. This allows minute amounts of material to be placed on the surface of the rolls and then milled using the Excimer laser to the specifications of the design. This offers the best of both material removal and addition techniques. However, the costs increase significantly for this approach due to the increase in production time.

5.1.4 Focused Ion Beam

Focused ion beam (FIB) is another non-traditional machining type that uses energy to remove material from a workpiece. But while laser ablation uses pulses to heat and sublimate material, FIB sputters atoms form the surface of the workpiece due to the momentum of the ions in the beam. Because individual atoms are being removed from the surface of the material, structures as small as 50 nm can be created. The surface quality is also much higher using this process than any of the other processes described here [27]. And like laser processing, FIB can also add material to the surface. But this material can be added much more precisely through FIB, eliminating the need to mill the material after deposition [37]. Material deposited with this method can be three dimensional as well, as seen in Figure 5-3, increasing the flexibility of this roller processing technique.

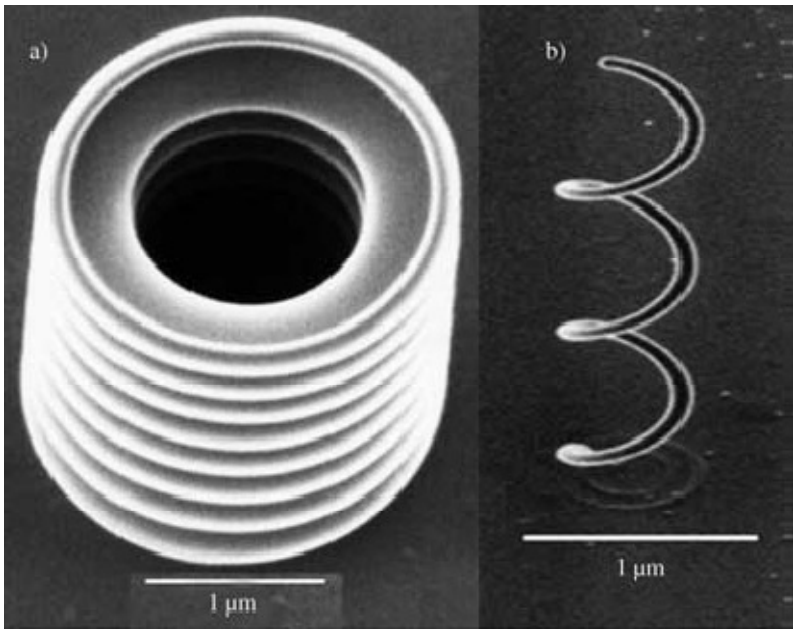

Figure 5-3 – FIB 3-D capabilities. a) Microbellows with a 100 nm thickness, 800 nm pitch, 2.75 µm external diameter and 6.1 µm height. b) Microcoil with a 600 nm coil diameter, 700 nm coil pitch and 80 nm wire diameter. Adapted from [37].

5.2 Material Addition Fabrication Techniques

Techniques described within this section will deal with methods to precisely add material to the virgin rollers. In all cases, the material added will not be of the same material the virgin roller is made from, and in many cases not even a metal. This could lead to durability issues as the material added will not be as strong as the roller material and therefore the surface can be damaged much more easily. However, the major advantages to these methods are the significant decrease in fabrication speed (or lead time in the case of contracting it out) and cost. Another drawback is the accuracy and precision attainable through these methods. However, the costs of these techniques are more than an order of magnitude less than the previous techniques described.

5.2.1 Electroplating

Electroplating is performed by running a current through conductive material to remove cations from a solution. These cations form a thin layer on the exposed conductive areas of the workpiece. For the experiments run with this system, a modified LIGA process [38] was used. This process involves coating the virgin rollers with a photoresist (SU-8) and patterning it using photolithography to limit the conductivity to areas desired. After electroplating for a certain amount of time based on the desired thickness, the SU-8 on the rolls must be are removed. What is left is the final product that has a nickel coating in the areas designated by the original pattern. Figure 5-4 shows an optical microscopy image of one of the rolls used in these experiments.

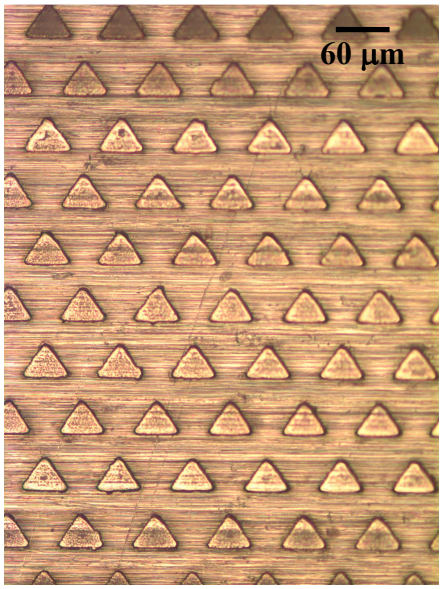

Figure 5-4 – Microscopy image of roll created by electroplating. The base roll is stainless steel with nickel electroplated to form the pattern seen. Courtesy of University of Kentucky Bearings and Seals Lab.

5.2.2 Taping

The taping method is by far the simplest conceptual method of roll fabrication described in this thesis. This technique is very similar to a group that used a vinyl sign plotter to create microfluidic channels [39]. In this method, high temperature oven tape that has been laser cut with the desired pattern is applied to the virgin rolls. The limits of this technology are the thickness of the oven tape and the accuracy of the laser cutter used. Results using a VersaLaser 2000 and a polyimide tape of 0.2 mm thickness showed the smallest feature size to be 0.5 mm. Although this is not technically a microfabrication technique, it takes much less time than any other technique described and can be changed in a few minutes. The accuracy of the edge features was also not ideal in these experiments. Patterns that were designed to be circular sometimes ended up as ovals and it was clear that the laser was not designed to cut through the adhesives. Figure 5-5 shows an optical microscopy image of PDMS from the experiments performed using these rolls. However, using a stronger and more accurate laser, it may be possible to achieve much better results using this process.

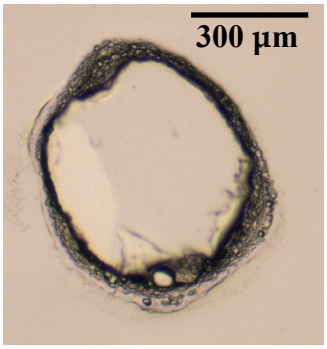

Figure 5-5 – Microscopy image of PDMS created using taping method. This 0.5 mm diameter circular pattern (smallest pattern available with Versa Laser used) was distorted into an oval shape. With a more precise laser specifically designed to cut adhesives, better results may be possible.

5.2.3 Wrapping (R2RNIL Method)

The wrapping method is the technique used in roll-to-roll nano-imprint lithography [7, 8]. An ETFE mold is created by hot embossing a film of ETFE with a pattern from an etched silicon chip. The ETFE is then cut to size and applied to a stainless steel roller using double sided tape, as shown in Figure 5-6. The major drawback to using this method with the continuous casting system is the fact that the materials used will all have different thermal coefficients of expansion. The pattern could shift slightly and cause defects. A way to avoid this is to apply the mold to the roller while hot. The advantage to this system is its accuracy, speed and the fact that the virgin roller does not have to be surface treated initially. This is a huge advantage in not only in cost, but in surface roughness of the final product as the ETFE film should have the same surface roughness of the silicon chip it was created from which can be as low as 0.01 μm Ra [40]. However, it is a multistep process that requires use of a hot embossing machine.

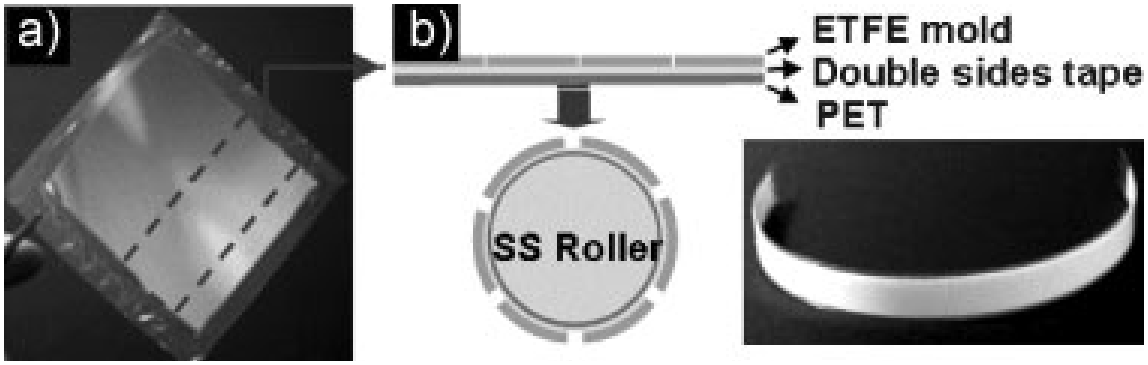

Figure 5-6 – Creation of roller using the wrapping method. a) A flexible ETFE mold is created from a silicon master. b) The mold is prepped and applied to a stainless steel roller. The PET layer is added for cushioning to assure conformal contact during the process. Adapted from [7].

5.3 Recommended Fabrication Technique

As shown in this chapter, there are several techniques available for manufacturing the rolls needed for this system. While the selection of manufacturing technique will depend heavily on the size and geometry of the desired features, there are several general suggestions that can be made. Obviously, the most recommended, and consequently most expensive, is using FIB technology. This is due to the flexibility (into or out of the roll), accuracy and surface roughness. However, if lead time and money is an issue, one of the material addition techniques would be a better alternative. The smallest lead time would be with the taping method, however, accuracy is limited. The choice between electroplating and wrapping comes down to availability of either a lab capable of performing the modified LIGA process or access to a micro-hot embossing machine. A more thorough comparison of these methods is listed in Table 5-1.

Table 5-1 – Comparison of each proposed manufacturing technique.

Manufacturing Processes	Description	Cost	Durability	Lead Time	Minimum Feature Size	Surface Roughness (R_a)	3-D Features
Micro Electro Discharge Machining	Features are created by a tiny spark discharged on the surface of the material. Very expensive process, but features are in bulk material of the roller and therefore very durable. Parts must be sent out to accomplish this and price will be based on a per feature base.	4	1	4	4 (5 μm [27])	5 (0.2 μm [31])	Yes
Traditional Micro Machining	Traditional machining, but using tiny tools (~10 micron diameter range and up). Also very expensive and has the same benefits and pricing scheme as above.	4	1	4	5 (25 μm [27])	4 (0.3 μm [29])	Yes
Laser Ablation	Laser beam is used to remove material from a solid surface. The heated material is either evaporated, sublimates or is turned into plasma. Depending on pulsing, very little heat will be transferred to surrounding area meaning extremely small features can be accurately replicated on the surface.	4	1	4	3 (2 μm [27])	6 (0.8 μm [35])	Yes
Focussed Ion Beam	Uses an ion beam to remove material due to the force of the ions impact with the substrate. Very similar to how an SEM works, but with ions instead that remove the material.	4	1	4	1 (50 nm [27])	3 (0.2 μm (roll limited))	Yes
Electroplating	Multi step method using a modified LIGA process. Thickness is limited by the electroplating procedure and the nickel formations do sometimes "flake" off of the base material. Features are created from a photomask and cost will be incurred per roller created, not per feature.	3	4	3	6 (30 μm)	7 (Electroplated Areas - 0.1 μm Roll Areas - 0.2 μm)	No
Taping	Oven tape is patterned out in a laser cutter and then wrapped around the surface. Tape does not last that long and current laser cutter only has capability of creating 500 micron holes.	1	6	1	7 (500 μm)	2 (Taped Areas - 5 nm Roll Areas - 0.2 μm)	No
Wrapping Method (R2RNIL)	This method is outlined in the [7] and involves creating a flat and patterned piece of ETFE and using double sided tape to attach it to a stainless steel roll.	2	5	2	2 (70 nm [7])	1 (0.01 μm from Silicone mold [40])	Yes

CHAPTER 6 – CONCLUSIONS AND FUTURE WORK

6.1 Conclusions

This machine could represent a significant step forward in the area of manufacturing PDMS with microstructures on its surface. The major barriers to commercialization are quality, quantity and cost. All three need to be combined into a singular system before manufacturers are going to buy into the field of microstructures. Many other systems offer quality, however lack the quantity and cost potential needed. Obviously, this has hurt the field in the way of commercialization as there are very few companies that offer microfluidic devices on the open market. The accuracy of this system—demonstrated through the profilometer scans—is comparable to conventional soft lithography techniques and the speed is shown to be almost an order of magnitude faster. From this, two of the three major hurdles were eliminated. Clearly this machine can accurately replicate microstructures on the surface of PDMS at an extremely fast rate.

The final challenge this system had to overcome was the cost factor. The machine surpasses current methods by moving away from batch processing and creating a continuous production line. This leads to a more consistent cycle time, less machine downtime and less user input. Combining these advantages significantly reduces cost per part, a major metric in the manufacturing world. Due to the limited user input, less experienced personnel can oversee the production of microfluidic devices, further reducing costs incurred by the manufacturer. This process also eliminates the need for use of a clean room or a highly-controlled operating environment. A combination of these

features makes this process a strong option for manufacturing microstructured PDMS materials.

6.2 Future Work

Despite the fact that this system overcomes the barriers to commercialization described, there are many areas of opportunity that future research with this process could significantly improve upon. These are listed below with brief descriptions of the opportunity and why it is needed. The order in which they appear does not correspond to their importance to the system.

1. Curvature of final product: the current size rolls (5.5" diameter) work extremely well with no curvature of the final product. However, smaller size rolls would have less surface area and therefore be less expensive to create, but how small is too small before the final product retains the curve of the roller. Several different size rolls would need to be tested before an accurate statement could be made, however, it is the author's opinion that the curvature of the final product would also depend on its thickness.

2. Machine Parameters: although speed, thickness and temperature charts were created and upper and lower limit formulas theorized, a more in depth study is needed. Figure 3-3 currently only uses 5 points to base each line. More points could be taken to confirm these limits and possibly characterize other major variables within the system.

3. Different Curing Materials: although PDMS is the standard material in use for microstructured devices, many other materials can be thermally cured with smaller shrinkage percentages. This system is not limited to PDMS, however it is currently

customized for it. Trials with other materials are needed to create new data points and parameters for these various other substances.

4. Roll Fabrication: chapter 5 of this thesis explains a variety of different methods that could be used to create the rollers; however experiments should be run to verify the fact that these methods could be used. This is the most expensive of the opportunities listed here, but worthwhile nonetheless due to the vast cost difference between the methods.

5. Thermal Analysis: further experiments and models should be performed to understand the mechanism of heat transfer from the rolls to the PDMS. This includes finding out the amount of energy needed to cure the PDMS.

6. Change PDMS: although a 10:1 is the recommended ratio of base to curing agent, other ratios could bring about different, possibly thinner, results. Also, to make the PDMS less viscous, mixing toluene with the base works and the toluene boils out during the curing process. This should be tested to see if it will cause defects.

7. Larger Aspect Ratios: larger aspect ratios features should be attempted to ensure that the rolls will not rip or tear the PDMS. The aspect ratio could also play a part in roll diameter selection.

Accomplishing just a few of the tasks listed above could help make this process a viable option for manufacturers.

APPENDIX A

Verification of Lumped Capacitance Assumption

To use the lumped capacitance method to calculate the temperature of a substance at any time, the Biot number of the substance needs to be less than 0.1 to assume a uniform temperature distribution across the solid. This appendix describes the application of the lumped capacitance assumption to the metal rollers used in this research during cooling from 190°C to room temperature. The following analysis is adapted from [41].

The Biot number is a ratio of the thermal resistance to conduction to the thermal resistance to convection across the fluid boundary layer. Using Equation A-1, the Biot number, *Bi*, is defined as the convective heat transfer coefficient, *h*, times the characteristic length, L_c, divided by the conductive coefficient of the material, *k*:

$$Bi = \frac{hL_c}{k} \tag{A-1}$$

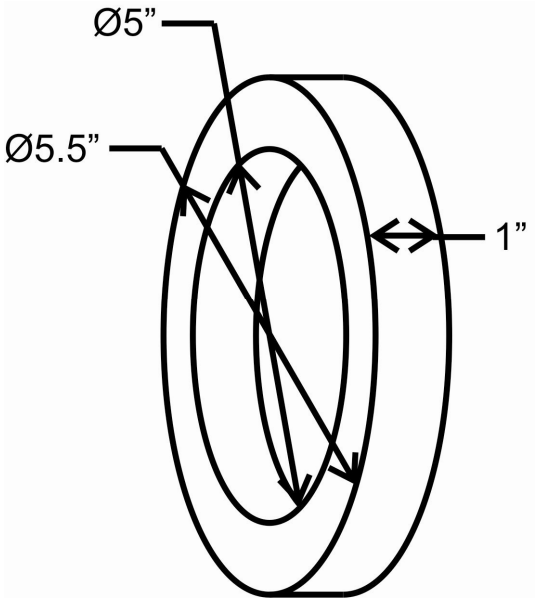

Figure A-1 – Roll dimensions used for calculations.

The characteristic length of the substance is based on Equation A-2 which is simply the volume of material, V, divided by the exposed surface area, A_s. Using the rollers in this research with the dimensions shown in Figure A-1, the characteristic length is 0.00345m:

$$L_c = \frac{V}{A_s} = 0.1358in = 0.00345m \tag{A-2}$$

To calculate the convective heat transfer coefficient, h, one can use Equation A-3 where k is the thermal conductivity of the material, D is the diameter of the rolls and Nu_D is the Nusselt number:

$$h = \frac{k}{D} Nu_D \tag{A-3}$$

The Nusselt number can be calculated through Equation A-4 where Ra_D is the Rayleigh number and Pr is Prandtl's number:

$$Nu_D = \left(0.6 + \frac{0.387 {Ra_D}^{1/6}}{\left(1 + \left(\frac{0.559}{Pr}\right)^{9/16}\right)^{8/27}} \right)^2 \tag{A-4}$$

The Rayleigh number is found using Equation A-5 where g is gravity, β is the thermal expansion coefficient, T_s is the surface temperature of the roller, T_{inf} is the temperature of the surrounding environment, D is the diameter of the roller, ν is the kinematic viscosity and α is the thermal diffusivity [41].

$$Ra_D = \frac{g\beta\left(T_s - T_{inf}\right)D^3}{\nu\alpha} \tag{A-5}$$

For air, ν = 22.8E-6 m^2/s, α = 32.8E-6 m^2/s and β = 2.725E-3 K^{-1} [41]. The temperature of the surface is 473K and the environment is 294K. Using a gravitational acceleration of 9.81 m/s^2 and the dimensions of the cylinder found in Figure A-1, Rayleighs number is found to be 1.7445E7.

Combining this result with a Prandtl number of 0.697 [41], a Nusselt number of 33.2529 is found using Equation A-4. Plugging this value into Equation A-3 along with the value of *k* for air (0.0313 W/m*K [41]) and the diameter of the roller as *D*, the convective heat transfer coefficient, *h*, is found to be 7.45 W/m^2K.

Using the thermal conductivity of stainless steel at 473K (*k* = 18.2 W/m*K [41]), the Biot number for this system using Equation A-1 is found to be 0.001412. Since this number is lower than 0.1, a lumped capacitance approach to this problem is allowable.

APPENDIX B

Derivation of Temperature Equation Using Lumped Capacitance Method

The following derivation was adapted from [41].

Fourier's law, when applied to a system where there is heat conduction in the absence of a temperature gradient, implies infinite thermal conductivity. This is impossible; however, if the rate that an object transfers heat to its surroundings is much smaller than the rate of thermal internal conduction, we can make the approximation of "infinite" thermal conductivity without incurring significant error. This approximation was used for calculations in Appendix A. By applying an energy balance to a solid with no energy input, the energy out of the system, $\dot{E}_{out}$, is equal to the energy change within the system, $\dot{E}_{stored}$:

$$-\dot{E}_{out} = \dot{E}_{stored} \tag{B-1}$$

Equation B-2 expands upon Equation B-1 in that the energy lost by the system is equal to the convective heat transfers and the energy stored is the heat capacitance of the system.

$$-hA_s\left(T - T_{inf}\right) = \rho V c \frac{dT}{dt} \tag{B-2}$$

In this case h is the convective heat transfer coefficient, A_s is the surface area, T is the starting temperature of the system, T_{inf} is the temperature of the surrounding environment On the right hand side of the equation ρ is the density of the material, V is the volume, c is the heat capacitance and dT/dt is the change in temperature of the solid over time. For

the sake of convenience, a temperature differential, θ, shown in Equation B-3 can be introduced:

$$\theta = T - T_{inf} \tag{B-3}$$

Using the temperature differential, it can be easily shown in Equation B-4 how to the temperature gradient is equal to the temperature differential gradient.

$$\frac{d\theta}{dt} = \frac{dT}{dt} \tag{B-4}$$

To properly assess the equations, an initial temperature differential, θi, must be assigned as shown in Equation B-5 where T_i is the initial temperature and T_{inf} is the reservoir temperature.

$$\theta_i = T_i - T_{inf} \tag{B-5}$$

Combining Equation B-2 with these new variables and integrating both sides from the initial time point results in Equation B-6:

$$\frac{\rho V c}{h A_s} \int_{\theta_i}^{\theta} \frac{d\theta}{\theta} = -\int_{0}^{t} dt \tag{B-6}$$

Completing the integration of Equation B-6 leads to Equation B-7:

$$\frac{\rho V c}{h A_s} ln\left(\frac{\theta}{\theta_i}\right) = -t \tag{B-7}$$

This can be rearranged to form Equation B-8:

$$\theta = \theta_i e^{-\left(\frac{hA_s}{\rho Vc}\right)t} \tag{B-8}$$

Substituting back in for the temperature differentials, the previous equation can be rearranged to form Equation B-9:

$$T(t) = T_{inf} + \left(T_i - T_{inf}\right)e^{-\left(\frac{hA_s}{\rho Vc}\right)t} \tag{B-9}$$

To find the final equation for temperature at any given time (Equation B-10), the constant h = 7.45 W/m^2*K, ρ = 1670 kg/m^3 and c=s 536 J/kg*K [41]. The initial temperature of the rollers (473K), the reservoir temperature (296K) and the conditions imposed by the geometry of the rollers (found in Figure A-1) were also applied to yield:

$$T(t) = 296K + (177K)e^{-0.000804t} \tag{B-10}$$

APPENDIX C

Machine Budget[1]

Machine Area	Company	Part	Price	Area Price
Motor				
	Grainger	DC Motor	$261.90	
		Motor Controller	$115.92	
	McMaster	Timing Belt	$11.85	
		Timing Pulley	$32.04	
				$377.82
Roller Mounts				
	McMaster	Bearings	$117.96	
		Shaft Collars	$53.20	
				$171.16
Frame				
	Machine Shop	Base Plate	$840.00	
		Moving Frame	$780.00	
		Frame Tops	$180.00	
	Deltron	Precision Stage	$346.00	
	McMaster	Mounting Hardware	$6.76	
				$2,152.76
Internal Heating				
	Omega	Heat Tape	$98.00	
		Controller	$88.00	
	Moog	Slip Ring	$280.60	
				$466.60
			Total Machine Cost (minus rolls)	**$3,168.34**

[1] Frame and internal heating budget numbers are estimated from a local machine shop, Omega and Moog as these items were not purchased for the prototype.

APPENDIX D

Orifice Dimensions Used in Figure 3-2

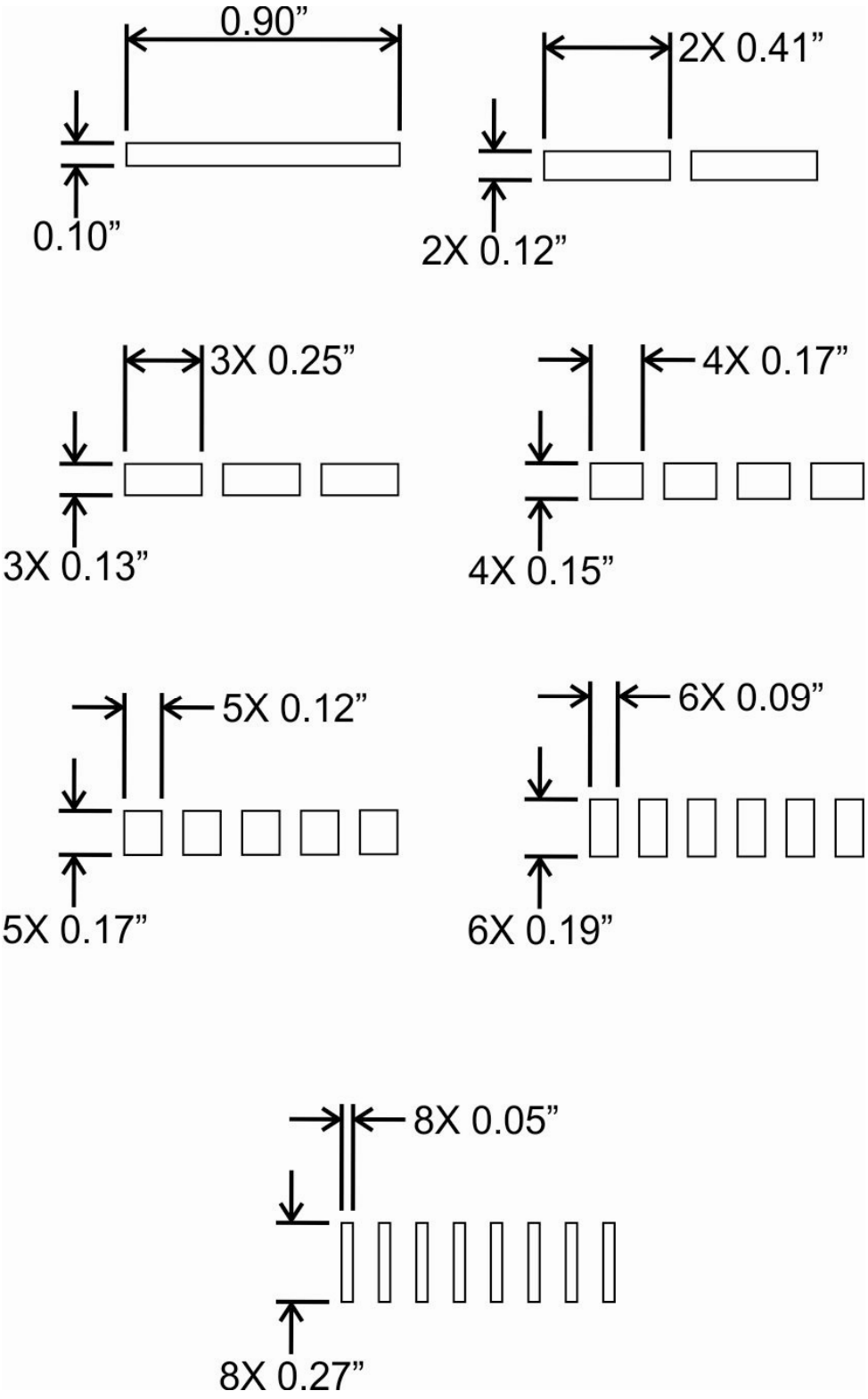

APPENDIX E

Description of line contact experiment

The line contact strength of PDMS bonded against stainless steel was determined experimentally. The experiment consisted of the setup seen in Figure D-1, where a wire was embedded in PDMS and attached to a force gauge. The force needed to remove the PDMS at a constant speed from the experimental setup was shown to a have a line contact strength of 0.15 N/mm along the axis into and out of the page.

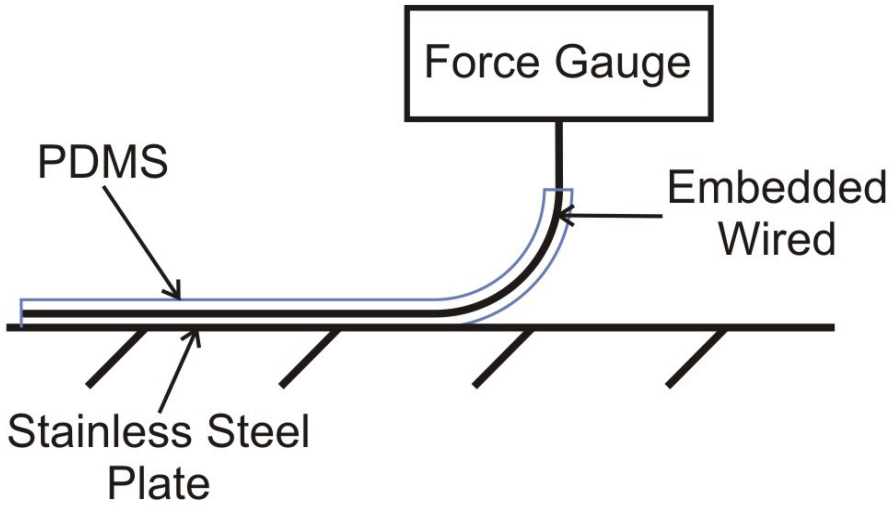

Figure D-1 – Experimental setup used to measure line contact strength of cured PDMS bonded on stainless steel. The axis measured is into and out of the page

APPENDIX F

Derivation of the radiation heat transfer coefficient

The radiation heat transfer coefficient, h_{rad}, is defined by Equation E-1 where ε is the emissivity of the surface, σ is the Stefan-Boltzmann constant, T_s is the surface temperature and T_{sur} is the temperature of the surroundings [41]:

$$h_{rad} = \varepsilon\sigma(T_s + T_{sur})\left({T_s}^2 + {T_{sur}}^2\right) \quad \text{(E-1)}$$

Applying values of 5.67E-8 W/m^{2}K^4 for σ, 0.18 for ε [41], 473 for T_s and 296 for T_{sur} gives a radiative heat transfer coefficient, h_{rad}, of 2.44W/m^{2}K.

APPENDIX G

Roller Design sent for quoting

Each pattern was to be repeated four times at depths of 1, 5, 10 and 20 μm. All dimensions shown are in mm.

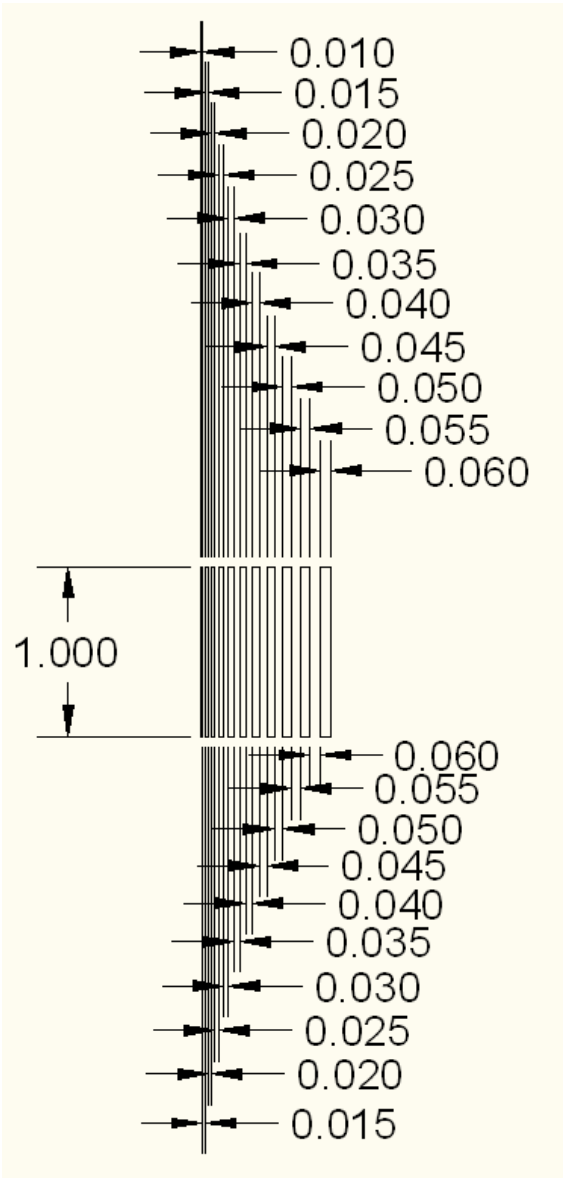

Figure F-1 – Simple line pattern designed to test roller fabrication method accuracy and reliability. This pattern was also created at rotation angles of 45^{o} and 90^{o}.

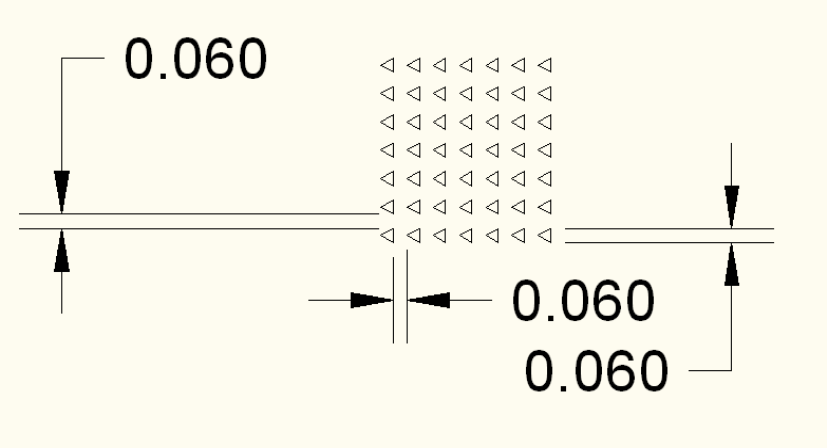

Figure F-2 – Triangle pattern used for comparison to electroplated rollers.

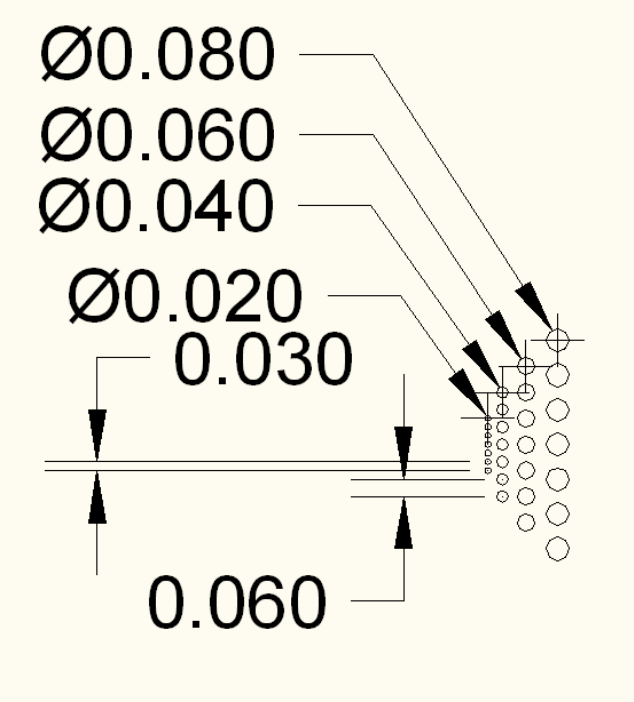

Figure F-3 – Circle pattern

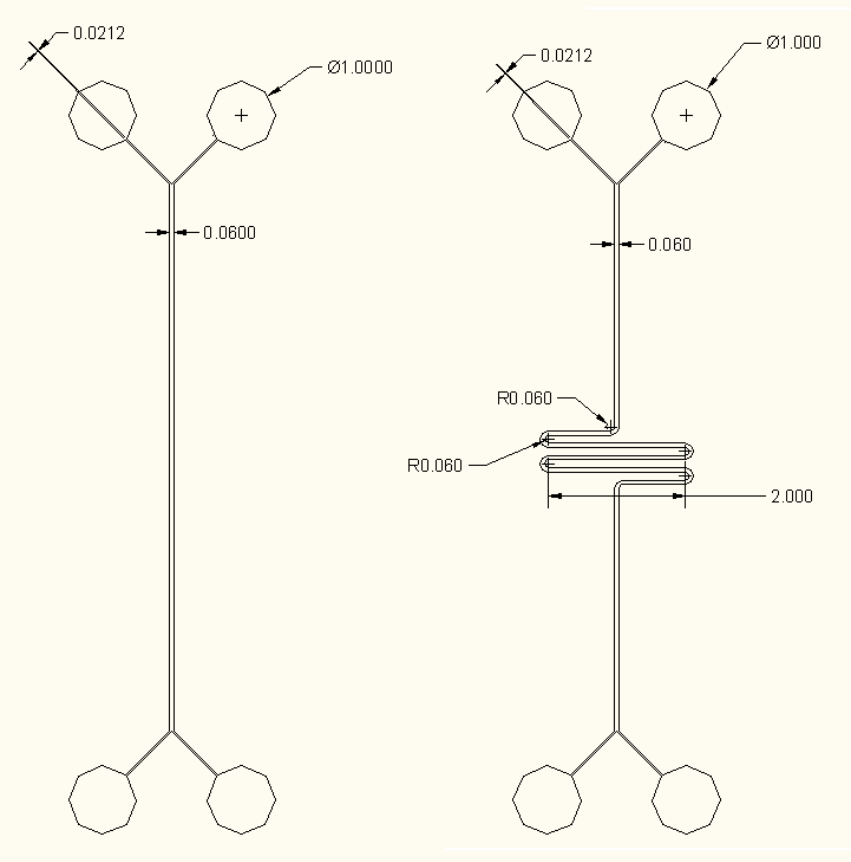

Figure F-4 – Straight (left) and curved (right) micromixer.

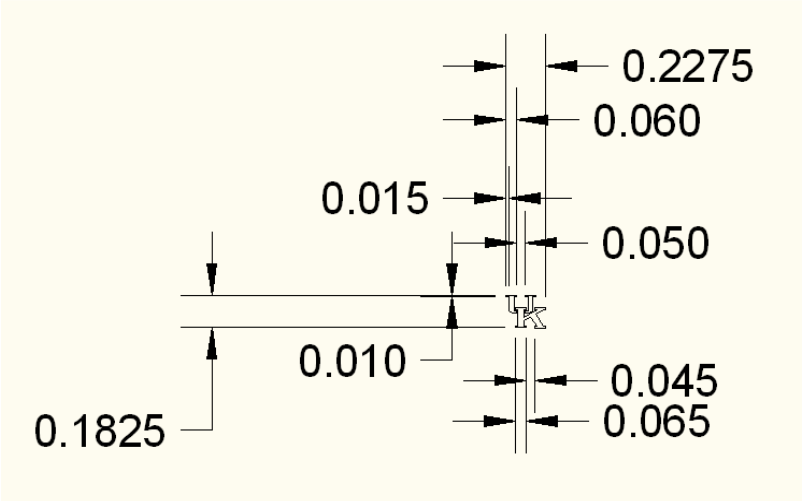

Figure F-5 – Complex symbol to test capabilities of fabrication system.

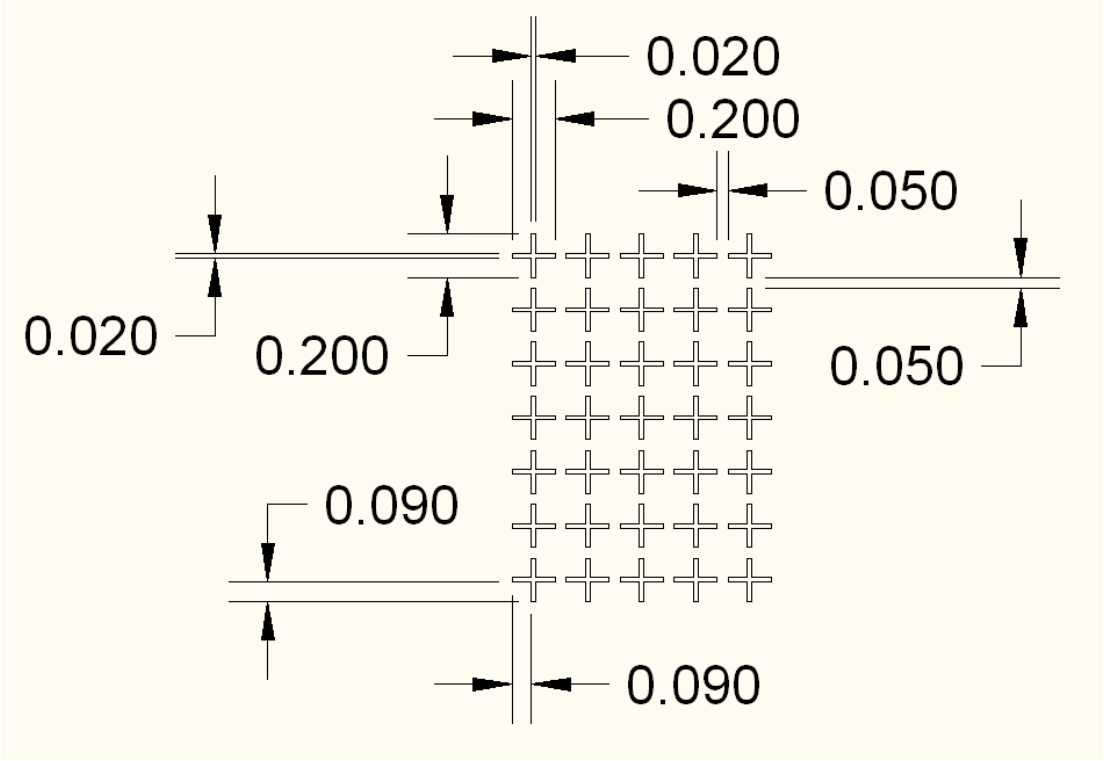

Figure F-6 – Cross pattern

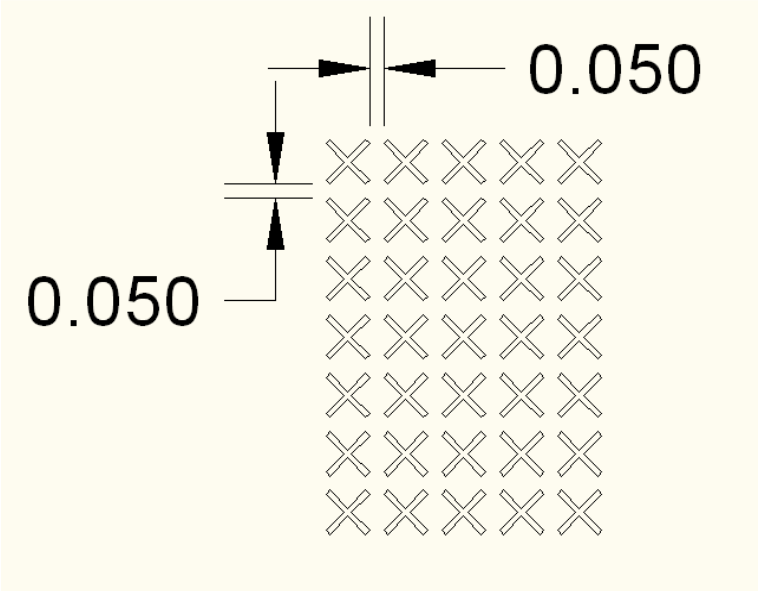

Figure F-7 – Pattern of "X"s with same dimensions as crosses rotated by 45^{o}.

REFERENCES

1. McDonald, J.C., et al., *Fabrication of microfluidic systems in poly(dimethylsiloxane).* Electrophoresis, 2000. **21**(1): p. 27-40.

2. Whitesides, G.M., *The origins and the future of microfluidics.* Nature, 2006. **442**(7101): p. 368-373.

3. Becker, H., K. Lowack, and A. Manz, *Planar quartz chips with submicron channels for two-dimensional capillary electrophoresis applications.* Journal of Micromechanics and Microengineering, 1998. **8**(1): p. 24-28.

4. Sire, J.Y., Marin, S. and Allizard, F., *Comparison of Teeth and Dermal Denticles (Odontodes) in the Teleost Denticeps Clupeoides (Clupeomorpha).* Journal of Morphology, 1998. **237**: p. 237-255.

5. White, S.R., et al., *Autonomic healing of polymer composites.* Nature, 2001. **409**(6822): p. 794-797.

6. Duffy, D.C., et al., *Rapid prototyping of microfluidic systems in poly(dimethylsiloxane).* Analytical Chemistry, 1998. **70**(23): p. 4974-4984.

7. Ahn, S.H. and L.J. Guo, *High-speed roll-to-roll nanoimprint lithography on flexible plastic substrates.* Advanced Materials, 2008. **20**(11): p. 2044-+.

8. Ahn, S.H. and L.J. Guo, *Large-Area Roll-to-Roll and Roll-to-Plate Nanoimprint Lithography: A Step toward High-Throughput Application of Continuous Nanoimprinting.* Acs Nano, 2009. **3**(8): p. 2304-2310.

9. Terry, S.C., J.H. Jerman, and J.B. Angell, *Gas-Chromatographic Air Analyzer Fabricated on a Silicon-Wafer.* Ieee Transactions on Electron Devices, 1979. **26**(12): p. 1880-1886.

10. Fan, Z.H. and D.J. Harrison, *Micromachining of Capillary Electrophoresis Injectors and Separators on Glass Chips and Evaluation of Flow at Capillary Intersections.* Analytical Chemistry, 1994. **66**(1): p. 177-184.

11. Whitesides, G.M. and A.D. Stroock, *Flexible methods for microfluidics.* Physics Today, 2001. **54**(6): p. 42-48.

12. Becker, H. and C. Gartner, *Polymer microfabrication methods for microfluidic analytical applications.* Electrophoresis, 2000. **21**(1): p. 12-26.

13. Martynova, L., et al., *Fabrication of plastic microfluid channels by imprinting methods.* Analytical Chemistry, 1997. **69**(23): p. 4783-4789.

14. Becker, H. and U. Heim, *Hot embossing as a method for the fabrication of polymer high aspect ratio structures.* Sensors and Actuators a-Physical, 2000. **83**(1-3): p. 130-135.

15. McCormick, R.M., et al., *Microchannel electrophoretic separations of DNA in injection-molded plastic substrates.* Analytical Chemistry, 1997. **69**(14): p. 2626-2630.

16. Ng, J.M.K., et al., *Components for integrated poly(dimethylsiloxane) microfluidic systems.* Electrophoresis, 2002. **23**(20): p. 3461-3473.

17. Xia, Y.N. and G.M. Whitesides, *Soft lithography.* Annual Review of Materials Science, 1998. **28**: p. 153-184.

18. *Sylgard 184 silicone elastomer kit*. [Website] 2010 [cited 2010 21 July].

19. DiBartolomeo, F.a.T., Christine, *High Throughput Continuous Fabrication of Large Surface Area Microstructured PDMS*, in *Proc. of the ASME 2009 International Mech. Eng. Congress and Exposition*2009, ASME: Lake Buena Vista, FL.

20. Stephens, L.S., et al., *Deterministic micro asperities on bearings and seals using a modified LIGA process.* Journal of Engineering for Gas Turbines and Power-Transactions of the Asme, 2004. **126**(1): p. 147-154.

21. Corp., D. *Plastic Properties of Acrylonitrile Butadiene Styrene (ABS)*. 2010 [cited 2011 11 March]; Available from: http://www.dynalabcorp.com/technical_info_abs.asp.

22. *SRT Heating Tapes*, 2010, Omega Engineering Inc.: Stamford, CT.

23. Gutowski, T.G., et al., *Thermodynamic Analysis of Resources Used in Manufacturing Processes.* Environmental Science & Technology, 2009. **43**(5): p. 1584-1590.

24. Liu, M., et al., *Thickness-dependent mechanical properties of polydimethylsiloxane membranes.* Journal of Micromechanics and Microengineering, 2009. **19**(3): p. -.

25. Technology, N.I.o.S.a., *Poly(dimethylsiloxane)*, 2008, NIST.

26. Schey, J.A., *Introduction to Manufacturing Processes*. 3rd ed2000, New York: McGraw Hill.

27. Brousseau, E.B., S.S. Dimov, and D.T. Pham, *Some recent advances in multi-material micro- and nano-manufacturing.* International Journal of Advanced Manufacturing Technology, 2010. **47**(1-4): p. 161-180.

28. Chae, J., S.S. Park, and T. Freiheit, *Investigation of micro-cutting operations.* International Journal of Machine Tools & Manufacture, 2006. **46**(3-4): p. 313-332.

29. Uriarte, L., et al., *Comparison between microfabrication technologies for metal tooling.* Proceedings of the Institution of Mechanical Engineers Part C-Journal of Mechanical Engineering Science, 2006. **220**(11): p. 1665-1676.

30. Masaki, T., Kawata, K, and Masuzawa T., *Micro Electro-Discharge Machining and Its Applications.* Micro Electro Mechanical Systems, 1990. Proceedings, An Investigation of Micro Structures, Sensors, Actuators, Machines and Robots. IEEE 1990: p. 21-26.

31. Liu, K., B. Lauwers, and D. Reynaerts, *Process capabilities of Micro-EDM and its applications.* International Journal of Advanced Manufacturing Technology, 2010. **47**(1-4): p. 11-19.

32. Pham, D.T., et al., *Laser milling.* Proceedings of the Institution of Mechanical Engineers Part B-Journal of Engineering Manufacture, 2002. **216**(5): p. 657-667.

33. Pham, D.T., et al., *Laser milling as a 'rapid' micromanufacturing process.* Proceedings of the Institution of Mechanical Engineers Part B-Journal of Engineering Manufacture, 2004. **218**(1): p. 1-7.

34. Heyl, P., T. Olschewski, and R.W. Wijnaendts, *Manufacturing of 3D structures for micro-tools using laser ablation.* Microelectronic Engineering, 2001. **57-8**: p. 775-780.

35. Karnakis, D.M., Knowles, M.R.H., Petkov, P.V., Dobrev, T. and Dimov, S.S., *Surface integrity optimisation in ps-laser milling of advanced engineering materials*, in *Proceedings of Fourth International WLT-Conference on Lasers in Manufacturing*2007, Wissenschaftliche Gesellschaft Lasertechnik, e.V.: Munich.

36. Choi, D.S., et al., *Development of a direct metal freeform fabrication technique using CO2 laser welding and milling technology.* Journal of Materials Processing Technology, 2001. **113**(1-3): p. 273-279.

37. Tseng, A.A., *Recent developments in nanofabrication using focused ion beams.* Small, 2005. **1**(10): p. 924-939.

38. Venkatesan, S., *Surface Textures For Enhanced Lubrication: Fabrication And Characterization Techniques*, in *Mechanical Engineering*2005, University of Kentucky: Lexington.

39. Armani, M., Probst, R and Shapiro, B, *Fabrication PDMS Microfluidic Channels Using a Vinyl Sign Plotter*, in *Lab on a Chip Technology (Vol. 1): Fabrication and Microfluidics*, K.E.a.R. Herold, A, Editor 2009, Caister Academic Press: Norfolk, UK. p. 9-15.

40. Koshimizu, S., *Measurement of surface roughness and thickness of silicon wafers using an infrared laser.* Advances in Abrasive Technology Viii, 2005. **291-292**: p. 377-380.

41. Incropera, F.P.a.D., D.P., ed. *Introduction to Heat Transfer*. 3rd ed. 1996, John Wiley & Sons: New York.

VITA

Franklin John DiBartolomeo

Born October 28, 1983 in Hackensack, New Jersey, USA.

Education:

Bachelor of Science in Mechanical Engineering, 2007

Rochester Institute of Technology, Rochester, New York, USA

Professional Positions:

Technical Editor, Drag Racing Action Magazine, October 2007 – Present

Beaver Springs, Pennsylvania, USA

Product Engineer, Lexmark International Inc., August 2007 – August 2008

Lexington, Kentucky, USA

Professional Membership:

Student Member, American Society of Mechanical Engineers (ASME)

Professional Publications:

- DiBartolomeo, F., Trinkle, C., (2009), "High Throughput Continuous Fabrication of Large Surface Area Microstructured PDMS", *Proceedings of the 2009 ASME International Mechanical Engineering Conference and Exposition*, Lake Buena Vista, Florida, USA.